

Review

# A Review of Passive Constant Flow Regulators for Microfluidic Applications

Eric Chappel 

Debiotech SA, 28 Avenue de Sévelin, 1004 Lausanne, Switzerland; e.chappel@debiotech.com

Received: 20 November 2020; Accepted: 7 December 2020; Published: 10 December 2020



**Abstract:** This review gives an overview of passive constant flow regulators dedicated to microfluidic applications. Without external control and energy consumption, these devices deliver a constant flow rate regardless of pressure variations, making them very attractive for various microfluidic applications, including drug delivery, flow chemistry, point-of-care tests, or microdialysis. This technical review examines progress over the last three decades in the development of these flow regulators and focuses on the working principle, fabrication methods, performance, and potential applications.

**Keywords:** passive flow regulator; flow control valve; microfluidics; microsystems; microvalves; MEMS; lab-on-a-chip; diagnosis; hydrocephalus shunt; drug delivery

## 1. Introduction

Passive flow control regulators, also known as passive flow control or autoregulated or pressure-compensated valves, deliver a constant flow rate regardless of pressure variations. These valves are widely used in industry for water treatment, process water control (limiting peak flow rate), water authorities (flow limiting, boost mains pressure), centrifugal pump protection, water-saving (domestic showers, drinking fountains), irrigation, etc. [1,2]. These valves are compact, reliable, maintenance-free, and require no energy. Manufacturers (e.g., Maric Flow Control, Tokyo Keiso, Plast-o-Matic, Flowmate, the Lee Corporation, Parker Hannifin, etc.) provide passive valves dedicated to high flow rate (from a few hundred mL/min to 10,000 L/min and more) and large pressure differential (from 1 bar to several hundreds of bar). In this review, a focus is made on passive constant flow valves dedicated to microfluidic applications, including drug delivery, flow chemistry, point-of-care tests, hydrocephalus treatment, microdialysis, etc. These passive flow regulators fall into two main categories: the mechanical regulators having moving parts (a membrane in silicon or elastomer, a piston, a collapsible tubing, or a flap), and non-mechanical regulators without moving parts (fixed geometry), wherein the rheological properties of the fluid are exploited to achieve a constant flow rate. Most of the regulator designs analyzed in this survey belong to the first category. The automatic adjustment of the flow rate with varying pressure conditions is obtained by a change of the fluidic pathway dimensions. A variation of pressure moves a flexible element of the passive flow regulators to induce a change of the fluidic pathway cross-section in almost all configurations except the device with a spiral groove onto a moving piston and the device with a flexible silicon (Si) membrane and a spiral-shaped channel, wherein the length of the channel is automatically adjusted. This classification of the passive constant flow regulators dedicated to microfluidic applications, illustrated in Figure 1, is partly derived from the system set forth by Laser and Santiago for micropumps [3]. The review surveys progress over the last three decades in the development of these passive constant flow regulators. The working principle and performance of each device are discussed, along with a description of the fabrication process and the potential applications.

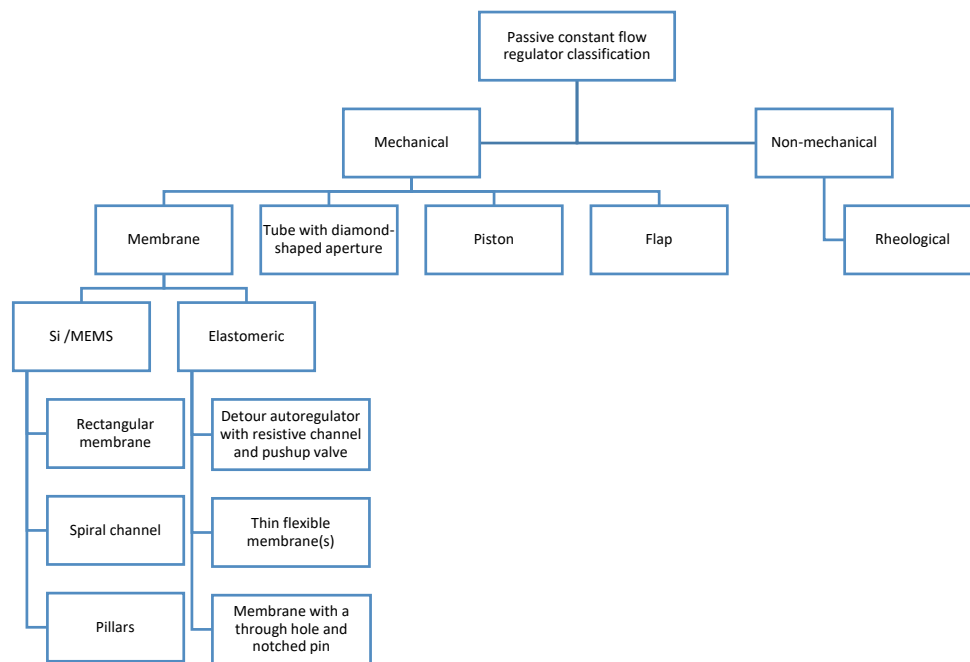


**Figure 1.** Classification of the passive constant flow regulators dedicated to microfluidic applications.

## 2. Passive Constant Flow Regulators—General Considerations

### 2.1. Working Principle

The passive constant flow regulators considered in this review are related to microfluidics, which refers to the manipulation of fluids in channels or structures with dimensions of tens of micrometers [4]. By contrast to macroscopic fluids, viscosity is more important than inertia, and the Reynolds number ( $Re$ ) that characterizes the ratio of inertial to viscous forces on the fluid is usually lower than 2000 in most microfluidic systems. The flow in such microstructures is in the laminar regime with highly predictable fluid dynamics. The estimation of the hydraulic resistances along the fluid pathway is done using the governing equations of laminar viscous fluid flow (see, e.g., References [5,6]). A constant passive flow regulator is intended to deliver a constant flow rate,  $Q_0$ , in a predefined pressure gradient range comprised between  $\Delta P_{reg\ min}$  and  $\Delta P_{reg\ max}$ , as illustrated in Figure 2. Further increasing the pressure gradient between the inlet and the outlet can, depending on the regulator design and the target application, either stops the flow rate (passive shut-off feature) or generates a flow rate larger than  $Q_0$ , the nominal flow rate.

At a given temperature  $T$ , the flow rate  $Q$  in the flow regulator is:

$$Q = \frac{\Delta p}{R_h} \tag{1}$$

where  $\Delta p = P_{out} - P_{in}$  is the pressure drop between the inlet and the outlet of the device and  $R_h$  is the hydraulic resistance of the device. According to Figure 2, the hydraulic resistance is constant and equal to  $R_{h0} = \frac{\Delta P_{reg\ min}}{Q_0}$  if  $\Delta p \leq \Delta P_{reg\ min}$ . A further increase  $\delta p$  of the pressure gradient, with  $\delta p \leq \Delta P_{reg\ max} - \Delta P_{reg\ min}$ , induces an increase of the hydraulic resistance,  $\delta R_h$ . Using (1), we obtain:

$$\Delta P_{reg\ min} + \delta p = (R_{h0} + \delta R_h)Q_0 \tag{2}$$

and thus:

$$\frac{\delta R_h}{\delta p} = \frac{1}{Q_0} = Constant \tag{3}$$

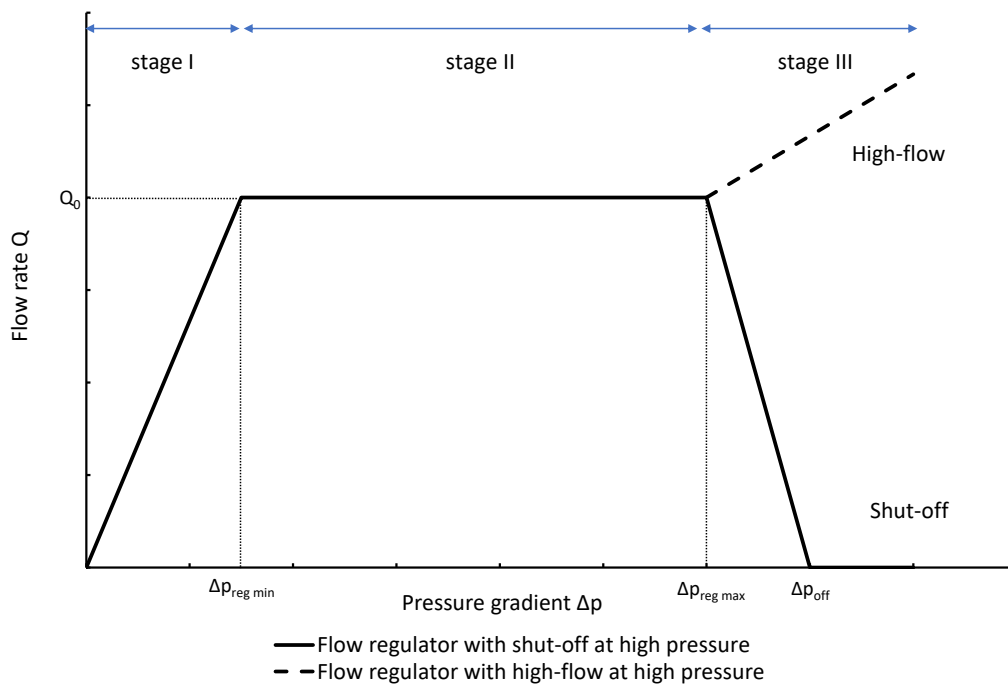


**Figure 2.** Ideal flow rate versus pressure gradient characteristic of a three-stage passive constant flow regulator. At low pressure (stage I), the regulator has a constant and low hydraulic resistance. In stage II, the flow is regulated at  $Q_0$  for a pressure gradient in the range  $[\Delta P_{\text{reg min}}; \Delta P_{\text{reg max}}]$ . At high pressure (stage III), the device could, according to its specific design, either stop the flow at  $\Delta P_{\text{off}}$  (solid line) or conversely, deliver a large flow rate (dashed line).

To maintain the flow rate constant in the gradient pressure range  $\Delta P_{\text{reg min}} \leq \Delta p \leq \Delta P_{\text{reg max}}$ , the hydraulic resistance of the passive regulator shall linearly increase with the pressure gradient up to  $\Delta P_{\text{reg max}}$ , where  $R_{fi}(\Delta P_{\text{reg max}}) = \frac{\Delta P_{\text{reg max}}}{Q_0}$ .

The change of slope in the  $Q(\Delta p)$  curve is representative of a nonlinear hydraulic resistor. At higher pressures, the regulator could further increase its hydraulic resistance until the flow is stopped or simply keep the hydraulic resistance constant (see Figure 2). A free-flow at high pressure can be obtained by fully by-passing the nonlinear resistor of the device (possible option for the piston spring valve [7]) or by adding a crack valve in parallel to the flow regulator (option implemented in the CRx Diamond Valve manufactured by Phoenix Biomedical Corp [8]).

The  $Q(\Delta p)$  profile shown in Figure 2 is, therefore, representative of a three-stage valve:

- Stage I—low-pressure stage, with low hydraulic resistance for  $\Delta p \leq \Delta P_{\text{reg min}}$
- Stage II—flow regulation stage, for  $\Delta P_{\text{reg min}} \leq \Delta p \leq \Delta P_{\text{reg max}}$
- Stage III—high-pressure stage, with a low or high hydraulic resistance for  $\Delta p > \Delta P_{\text{reg max}}$

The passive constant flow regulator is intended to be placed into a fluidic circuit. To keep the functioning point of the device onto the plateau of the  $Q(\Delta p)$  characteristic, it is recommended that the device exhibits the largest hydraulic resistance of the circuit.

An alternative method to maintain the flow rate at  $Q_0$  consists of the control of the pressure at the inlet of a flow restrictor. This method is exploited in constant flow rate implantable pumps for pain management (e.g., Infusaid-400, Medtronic Isomed, Codman 3000, Tricumed IP2000), wherein the reservoir pressure is generated by the vapor pressure of propellant (typically 2.5 bar), or in elastomeric pumps dedicated to ambulatory infusion of medication [6]. In both cases, a fluidic restriction (capillary) is used to set the flow rate in production, but the strategy to maintain the flow rate during the reservoir emptying is different. The propellant vaporizes progressively as the drug is infused toward the patient, while in the second type of device, the elastomeric balloon is designed

to keep the pressure almost constant during the treatment. A discussion of the flow rate accuracy of constant implantable pumps is provided by Dumont-fillon et al. [9]. For disposable and other portable infusion pumps, including devices powered by a spring, an elastomeric balloon, a chemical reaction, or a vacuum, overall flow rate accuracy of  $\pm 40\%$  was reported [10–12]. Also, these devices are sensitive to outlet pressure variations and temperature-induced change of the viscosity.

The combination of a pressurized reservoir and a passive constant flow regulator is recommended to avoid startup overflow and the constant decrease of the infusion rate over time as well. The infusion duration is better controlled and a flow rate error less than  $\pm 10\%$  can be achieved [9].

## 2.2. Working Fluid

Except for the device developed by Groisman et al. [13], almost all devices considered in this review were designed to work with water, cerebrospinal fluid (CSF), or other Newtonian fluids like viscous mixes of water and glycerol. In principle, the constant passive flow regulators are also compatible with gas. The modeling of a gas flow regulator can still be based on the standard continuum approach, which is still valid if no-slip boundary conditions apply, typically for Knudsen number  $Kn < 10^{-2}$  (viscous flow), where  $Kn$  is defined as the ratio of the fluid mean free path and the macroscopic length scale of the physical system [14].

In the laminar regime, a change of temperature induces a change of fluid viscosity which, in turn, leads to flow rate variability as for standard flow restrictors. Since the hydraulic resistance is proportional to the fluid viscosity  $\eta$ , the relative flow rate error is thus proportional to the opposite of the relative viscosity change with temperature, considering that the reference temperature is 20 °C:

$$Q(T) \propto \frac{1}{\eta(T)} \rightarrow \frac{Q(T) - Q(20^\circ\text{C})}{Q(20^\circ\text{C})} = -\frac{\eta_T - \eta_{20^\circ\text{C}}}{\eta_T} = \frac{\eta_{20^\circ\text{C}}}{\eta_T} - 1. \quad (4)$$

Table 1 shows, at selected temperatures, the relative flow rate error due to viscosity change. The values are derived from the empirical formula proposed by Kestin et al. for the dynamic viscosity of water in the range  $-8$  to  $+150$  °C [15]. Relative flow rate errors vary from  $-34\%$  to  $+53\%$  for operating conditions in the range  $[+5; +40]$  °C. It is noteworthy that additional error sources shall be considered to determine the passive flow regulator accuracy (e.g., fluctuations in the flow regulation stage, hysteresis).

**Table 1.** Effect of dynamic viscosity change with temperature on relative flow rate accuracy of passive constant flow regulators. The reference temperature is 20 °C.

Temperature (°C)	5	10	15	20	25	30	35	40
Water dynamic viscosity (mPa·s)	1.520	1.308	1.139	1.002	0.890	0.797	0.719	0.653
Relative water flow rate error (%)	-34.1%	-23.4%	-12.0%	0.0%	12.6%	25.7%	39.3%	53.5%

## 2.3. Materials

Silicon, glass, and poly(dimethylsiloxane) (PDMS) are the most common materials in contact with the working fluid in the passive constant flow regulators reported here. Titanium [7,16] was also considered for implantable devices. Early microfluidic and Micro Total Analysis Systems ( $\mu$ TAS) were made in glass and silicon due to the availability of process equipment and etching recipes. Since the Whitesides' group manufactured, in 1998, microfluidic devices in PDMS by soft lithography, PDMS became the preferred material for rapid prototyping of microchannel systems for use with biological samples [17–19]. Indeed, PDMS is an inexpensive, optically transparent, gas and vapor permeable, hydrophobic, relatively inert, and biocompatible polymer that, moreover, cures at low temperatures. PDMS is soft and facilitates removal from Si molds for micron-scale feature replication.

The surface energy of PDMS can be tuned to increase its wettability. Also, PDMS can be sealed reversibly to itself or other materials. Last but not least, the elasticity of PDMS has been widely exploited to create membrane pumps and check valves in active microfluidic devices for cell sorting and biochemical assays [20]. PDMS was also considered to make passive flow regulators because this material enables the rapid prototyping of complex three-dimensional (3D) structures. On the other hand, PDMS presents, compared to Si and glass, some disadvantages that can preterite its use as raw material for specific microfluidic applications that require long-term stability, reproducibility, well-controlled surface chemistry, high accuracy, stiffness, high temperature, compatibility with organic solvents, or low gas/vapor permeability. Si/glass biomedical electromechanical systems (BioMEMS) are more expensive to produce at low volume and require interconnections to the other parts of the fluidic systems. Silicon is a rigid material with a well-defined Young's modulus by contrast to the hyperelastic PDMS, whose mechanical properties are highly dependent on its degree of cross-linking and stretching. Si membranes exhibit a highly reproducible displacement and no fatigue, and the electronic properties of silicon enable the smart integration of reliable sensors [21]. Also, the negative charge surface of glass and silicon support electroosmotic flow (EOF).

#### 2.4. Modeling

The modeling of the passive constant flow regulator can be based on analytical models [7,22,23], but in a general way, 3D simulations using finite element methods are required to model the fluid–structure interactions (FSI) and the nonlinear behavior of membranes or flaps under large deformations. Numerical simulations are also useful to investigate the impact of machining tolerances on flow rate accuracy [9]. Specific tools using a genetic algorithm have been made to increase the yield in production by design optimization. This method was used to design a regulator with a flexible Si membrane that deflects against pillars. In addition to standard machining tolerances, other non-idealities have been introduced into the model, like wafer misalignment or valve tilt (due to particle contamination for instance) to increase the design robustness [22,24].

A passive flow regulator is usually part of a complex microfluidic system. In addition to these quasi-static analyses of the fluid flow in fixed pressure conditions, further simulations shall be carried out to calculate the fluid dynamics in a system that can include microchannels, check valves, micropumps, pressure sources, etc. As a passive flow regulator induces nonlinear effects, the equations governing the fluidic behavior of such systems generally have no analytical solutions. A classical approach consists of building an electrical equivalent network based on a subdivision of the system into lumped elements and the analogy between fluidic, mechanical, and electrical parameters [25,26]. The impedance of each element is estimated beforehand. For a passive flow regulator with an integrated check-valve, its electrical analog is a diode in series with a variable resistor. The analysis of the dynamics of complex systems can then be carried out very quickly with an electrical simulation tool. This method was chosen to simulate the dynamics of a hydrocephalus shunt comprising a passive flow regulator to divert CSF from the brain ventricles to the peritoneal cavity [27]. The ventricles are equivalent to a constant current source that produces about 20 mL of CSF every hour. The numerical model allowed the determination of the time evolution of intracranial pressure during patient postural changes, changes in the CSF formation rate, oscillations due to the vasogenic system, etc., together with a direct comparison with other shunt designs. Dynamic simulations based on electrical equivalent networks are particularly useful during the design phase to determine the behavior of the passive flow regulator. For a complex system such as the hydrocephalus flow control valve, the model can be further refined by the introduction of experimental data [28].

### 3. Mechanical Passive Constant Flow Regulators

The main characteristics of the passive constant flow regulators considered in this review are shown in Table A1 in Appendix A. Except for the nonlinear rheological devices made by Groisman et al. [13], all other devices fall into the first category of the classification: mechanical devices with moving parts.

The working principle of representative devices of the different subclasses, i.e., devices with Si or elastomeric membranes, a cylinder with a spiral groove, a tube with a lateral aperture, and a flap, is provided with a brief description of their performance and potential applications.

### 3.1. Devices with Flexible Membrane(s)

#### 3.1.1. Silicon Membrane(s)

##### Rectangular Si Membrane

To the best of the author's knowledge, the first passive constant flow regulator made using microelectromechanical system (MEMS) technology was conceived by Park et al. in 1988 for the treatment of hydrocephalus [29]. The device consists of a silicon wafer (membrane) between the top and bottom Pyrex covers. The rectangular Si membrane deflects, as the pressure increases, toward the bottom Pyrex cover to narrow the fluid path and therefore increase the hydraulic resistance (see Figure 3). Theoretical modeling of the membrane deflection and fluid flow was used to design the passive valve. The thin rectangular membrane was obtained by etching a 2" Si wafer. The top (inlet port) and bottom (outlet port) Pyrex covers were anodically bonded to the middle Si wafer. Tests performed with water showed a constant flow rate of about 0.015 mL/min in the pressure range [200; 400] mbar for the device with a channel height of 9.5  $\mu\text{m}$ , a membrane thickness of 26  $\mu\text{m}$ , and a ratio  $L/W = 2$ , where L and W are the channel length and width, respectively. The other design configurations did not show flow saturation. The saturation flow rate and pressure requirements for hydrocephalus (about 0.35 mL/min in the pressure range [10; 35] mbar) were not met, but the authors used the experimental data to refine the numerical model of this passive flow regulator with a thin rectangular membrane.

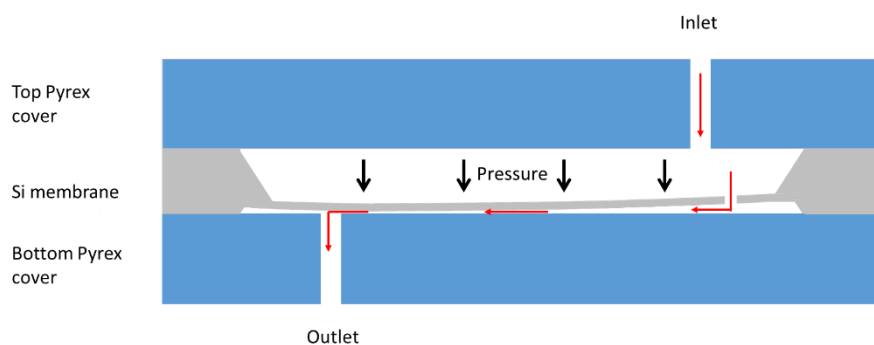


**Figure 3.** Schematic cross-section of a triple-stack passive flow regulator, with a Si wafer (membrane), bonded to the inlet and outlet Pyrex covers. The flow direction is indicated by red arrows. The fluid is forced to flow through the gap (or channel) between the membrane and the bottom cover that narrows as the pressure increases. As a result, the flow–pressure relationship becomes nonlinear.

##### Spiral Microchannels

In the device conceived by Park et al. [29], the channel cross-section varies continuously as the pressure changes since the channel is formed by the gap between the bottom of the moving membrane and the bottom cover. Considering also that the flow-induced pressure distribution along the channel leads to non-symmetrical membrane deformation, it must be stressed that the design of a constant flow regulator with such a structure is a challenging engineering task. An alternative passive flow regulator design comprising a well-defined channel cross-section was investigated by Amacker et al. at EPFL in 1998 [16] and further developed by Cousseau et al. at Debiotech SA in 2001 [30]. The device structure, shown in Figure 4, comprises an inlet port, a circular Si membrane with a central hole, a spiraling microchannel etched in a Pyrex substrate, and an outlet port. As the pressure difference between the inlet and the outlet increases, the Si membrane deflects and reduces the gap

between the membrane and the substrate. At low pressure, the main hydraulic resistance is due to the hole in the membrane. Once the membrane is in contact with the substrate, the fluid is forced to flow through the microchannel. The contact radius of the membrane with the substrate as a function of the pressure is obtained by finite element method (FEM) simulations since the membrane deflection is highly nonlinear. Constant microchannel cross-sections were considered in the two studies [16,30]. Therefore, constant flow regulation was achieved by calculating a spiral channel in a way that the part of the channel covered by the membrane increases linearly with the pressure. The target water flow rates of these passive devices for implantable drug delivery systems are 0.5 mL/day [16] and 1 mL/h [30].

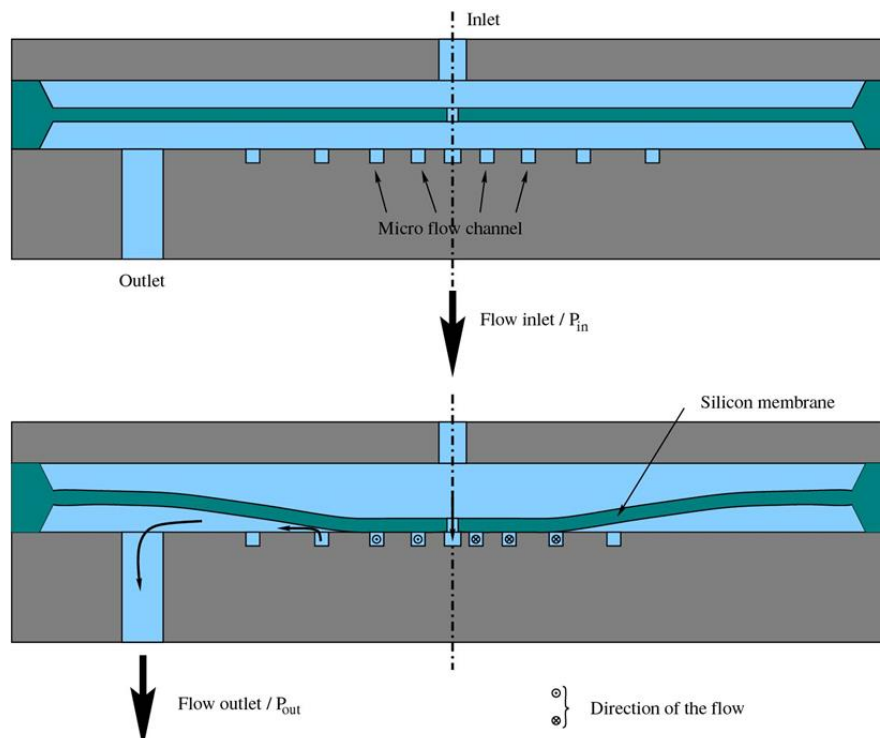


**Figure 4.** Cross-section of a triple-stack passive flow regulator, with a top Pyrex wafer (inlet port), a middle Si wafer (membrane), and a bottom Si or Pyrex wafer (substrate with a spiral microflow channel and an outlet port). As the pressure increases, the Si membrane deflects against the substrate and forces the fluid flow through the spiral channel. By design, the membrane covers a channel length that increases linearly with the applied pressure to maintain a constant flow rate (Courtesy of Debiotech SA, Switzerland).

Amacker et al. used a 45  $\mu\text{m}$  Si membrane with a hole of 20  $\mu\text{m}$  in diameter obtained by laser ablation. The channel in the glass substrate was etched in a 50% hydrofluoric acid (HF) solution. Finally, the membrane and the substrate were anodically bonded together. An alternative Titanium device was made of a stack of laser-drilled and electrochemically micromachined Ti sheets. A 20  $\mu\text{m}$  spacer ring was used to form the gap between the membrane and the substrate. The laminated Ti sheets were finally welded together. Water flow regulation at 5 nL/s (0.432 mL/day) was demonstrated in the pressure range [100; 600] mbar. At higher pressure, the flow increased beyond the regulation limit [16].

Cousseau et al. used a stack of three wafers: a top Pyrex wafer for fluidic connection, a central Si wafer for the membrane, and a bottom Si wafer for the microchannel substrate [30]. The membrane and the bottom channel are assembled, after structuration, by direct bonding, while the top wafer is anodically bonded to the membrane/substrate stack. After the determination of the contact radius of the membrane with the substrate as a function of the applied pressure, a 3D fluidic model was created and the program TASCflow was used to solve the incompressible Navier-Stokes equations.

Three different designs were tested using water with nominal flow rates of 0.85, 1.30, and 0.54 mL/h. The  $Q(\Delta P)$  profile of the 0.85 mL/h design showed, after a flow rate overshoot at low pressure (up to 2.5 mL/h), a constant water flow rate of 0.85 mL/h  $\pm$  5% in the pressure range [180; 500] mbar. At higher pressure, in the shut-off range [500; 800] mbar, the flow rate decreases progressively. Above 800 mbar, the channel is completely covered by the membrane and the flow is blocked. Long-term stability (26 days) and the ability to compensate for a sinusoidal pressure between 200 and 400 mbar were also demonstrated [30].

### Pillar Valves in Parallel

The passive flow regulators with a flexible Si membrane and a spiral microchannel required extended numerical simulations and are by design sensitive to particles, since the contact surface between the membrane and the substrate is large. Moreover, for square or semicircular microchannel cross-sections, flow rate varies as a power 4 with microchannel dimensions and the microchannel machining is a Critical-To-Quality (CTQ) process step due to the absence of etch stop. An alternative design made of a drilled Si membrane and a substrate with pillars, as shown in Figure 5, has been examined to overcome these abovementioned drawbacks [31]. A membrane hole and its facing pillar form a valve that closes progressively as the pressure increases. The resulting reduction of the gap between the top surface of the pillar and the bottom of the Si membrane leads to an increase in the hydrodynamic resistance of this radial valve. The valve modeling requires the determination, using 3D FEM simulations, of the membrane deflection and the fluid flow as a function of the pressure gradient. Simplified analytical models supported by experimental data were also used to simplify the design phase [32]. The total flow rate  $Q$  is the sum of the flows  $Q_i$  through each valve  $i$ :

$$Q = \sum_i Q_i = \frac{\Delta P}{\sum_i R_{h \text{ valve } i}} \quad (5)$$

where  $\Delta P$  is the pressure gradient between inlet and outlet and  $R_{h \text{ valve } i}$  is the hydraulic resistance of the valve  $i$ . To meet the targeted constant flow rate specification, a dedicated simulation tool based on a genetic algorithm has been developed to limit, by an optimization of the number of valves in parallel, their radial positions, the dimensions of the holes and pillars, etc., the impact of the machining tolerances on flow accuracy [22,24]. This regulator structure has been designed for CSF drainage [33] and drug delivery [22]. At high pressure, if each hole is associated with a facing pillar, all valves are closed and the flow is stopped. For the treatment of hydrocephalus, to prevent CSF accumulation and episodes of high intracranial pressure, the valve shall exhibit, as a safety feature, a low hydraulic resistance at high pressure. For this purpose, the specific regulator design includes a valve consisting of a pillarless hole to allow drainage of CSF at a high flow rate beyond the regulation range [33].

The passive constant flow regulator comprises a substrate made of glass or silicon, wherein the pillars and the outlet hole are machined, either by a combination of wet etch and sandblasting [30] or sequential dry etches [34]. The circular membrane with well-controlled thickness is obtained by dry etch of a silicon on insulator (SOI) wafer. Devices dedicated to low (respectively high) pressure applications have large and thin (respectively small and thick) flexible membranes. The final assembly consists of an anodic bonding of the two wafers (via a thin intermediate borosilicate layer for the Si-Si configuration [34]).

For the device dedicated to hydrocephalus, a constant flow rate of 13.5 mL/h at 20 °C (equivalent to 19.5 mL/h at 37 °C) was measured in the pressure range [50; 150] mbar using water [33]. Cornaggia et al. designed three different devices for the infusion of viscous fluids at high pressure, using thick SOI of 130  $\mu$ m, membranes with a diameter of 5.12 mm, and a water and glycerol mixture as working fluid [22]. For design A, a constant flow of 0.6 mL/min  $\pm$  5% was measured at 12 cP (or 12 mPa·s) in the pressure range [4; 21] bar. Designs B and C were tested using a 24 cP water/glycerol mixture and showed, respectively, a constant flow of 0.5 mL/min  $\pm$  5% in the pressure range [8; 21] bar and

0.13 mL/min  $\pm$  5% in the pressure range [7; 21] bar. Two similar device structures were tested by Conti et al., who reported constant flow rates of respectively 0.95 mL/min  $\pm$  5% in the pressure range [8; 19] bar and 0.21 mL/min  $\pm$  5% in the pressure range [6; 19] bar [34].

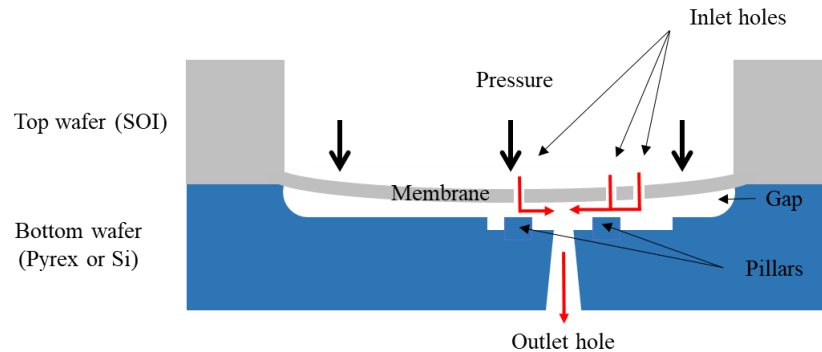


**Figure 5.** Cross-section of a passive flow regulator with a top SOI wafer (membrane) and a bottom wafer (substrate) made of Pyrex or Si. The fluid flows through the inlet holes of the membrane, the radial diffuser (annular restriction between the membrane and the pillar), and the outlet hole of the substrate. As the pressure increases, the deflection of the membrane induces an increase in the hydraulic resistance of the radial diffuser to keep the flow rate constant. The flow direction is indicated by red arrows.

Numerical simulations showed that flow rate variability due to the temperature dependence of the fluid viscosity can be mitigated by the use of a polyethylene block glued at room temperature beneath the pillar substrate made flexible by an additional backside etch [35]. This polyethylene (PE) block, which exhibits a large coefficient of thermal expansion of about  $200 \cdot 10^{-6} \text{K}^{-1}$ , is used as a passive thermal actuator that generates a large upward or downward force onto the substrate that respectively reduces or increases the gap between the membrane and the substrate as the temperature varies. A flow regulator delivering a constant water flow rate of 20 mL/h at 20 °C has been considered for the simulations. It was shown that the automatic adjustment of the gap due to the presence of the PE block keeps the flow constant at 20 mL/h  $\pm$  10% in the temperature range [+10; +30] °C and the pressure range [50; 150] mbar. Such a feature would improve the overall flow rate variability of a passive constant flow regulator used in an ambulatory infusion system.

The simulation tools specifically developed for this regulator design showed that for a target constant flow rate lower than 10 mL/h at 1 cP, the machining tolerances of the membrane hole diameters significantly narrow and become an important yield detractor in production. Infusion error larger than  $\pm 10\%$  at  $3\sigma$  could be expected [9]. To achieve a constant flow rate as low as 1 mL/day or less, Dumont-fillon et al. designed a triple-stack structure made of an SOI wafer to form a flexible membrane with no holes, a middle Si wafer with pillars, through holes and microchannels, and a bottom borosilicate wafer with inlet and outlet ports (see Figure 6) [9].

Flow regulation is again achieved by the deflection of a silicon membrane which gradually obstructs the fluid path as the pressure increases. The device has several valves in parallel, each valve consisting of an inlet port, a microchannel, a through hole in a pillar, and a radial diffuser (fluidic restriction between the top of the pillar and the bottom membrane). By contrast to the other elements of the valve, the hydraulic resistance of the radial diffusers varies with the pressure. The number of valves and their positions and dimensions are adjusted to meet the targeted fluidic characteristic of the passive constant flow regulator. At low pressure, the main hydraulic resistance is no longer a tiny hole but a long microchannel with a well-controlled cross-section obtained by anisotropic wet etch (potassium hydroxide (KOH)) of (100) Si wafers. A 50  $\mu\text{m}$  SOI with a 2  $\mu\text{m}$  buried oxide was used to form the circular membrane (3.5 mm in diameter). A 20  $\mu\text{m}$  borosilicate thick spacer was deposited to form the gap and to anodically bond the Si membrane wafer to the Si middle wafer. Two different devices dedicated to implantable infusion systems were designed to deliver a constant flow rate of 1 mL/h (High Flow (HF) design) and 1 mL/day (Low Flow (LF) design), respectively.

The samples were manufactured in a clean room and tested using water at 20 °C. The HF and LF samples exhibited a constant flow rate of 1 mL/h  $\pm$  10% and 1 mL/day  $\pm$  10% respectively, in the pressure range [200; 800] mbar. Replacing the fluidic restriction of a fixed-rate implantable pump by a passive constant flow regulator would enable a reduction in flow variability by up to a factor 2.4, and, for a safer refill procedure, a lowering of the reservoir pressure by a factor 5, from 2.5 to 0.5 bar [5,9].

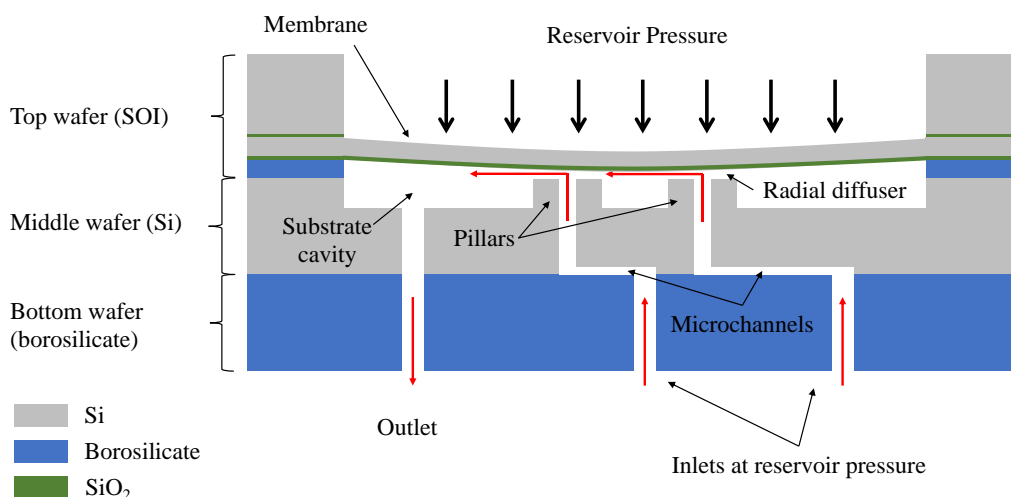


**Figure 6.** Schematic cross-section of a triple-stack microfluidic device dedicated to drug delivery at a constant flow rate of less than 10 mL/h, with a top SOI wafer (membrane), an intermediate borosilicate layer, a middle Si wafer (substrate) comprising pillars, through holes and microchannels, and a bottom borosilicate wafer with inlet and outlet ports. The top surface of the membrane and the inlet ports are in direct communication with the pressurized reservoir. The direction of the flow is indicated by red arrows. As the pressure increases, the gap between the membrane and the pillars (i.e., the radial diffusers) narrows and the hydraulic resistance of the device increases to keep the flow rate constant (adapted from Reference [9]).

### 3.1.2. Devices with Compliant Elastomeric Membrane(s)

In 2005, Yang et al. made early use of compliant PDMS membranes for the dynamic flow stabilization in microfluidic systems [36]. The device consists of a microchannel and PDMS membranes in series on one or more walls of the channel. The compliant membranes are equivalent to capacitors that are used to remove fluctuations in a pulsatile flow, and thus nearly constant outlet flow rates and pressure were obtained. To obtain a regulation of the flow rate at set pressures, other device structures were investigated. The present section of the review provides a detailed description of these passive devices that exploit the compliance of elastomeric membranes to achieve a constant flow rate under varying static pressure conditions.

#### Detour Autoregulator

Kartalov's group developed several detour autoregulatory devices in PDMS [37–39]. A schematic description of the working principle of these devices is provided in Figure 7. Pressure on the working fluid is applied at the inlet to produce a flow in the main channel of the upper layer. A detour channel is in fluidic connection with the main channel and through a via with a pushup valve located in the lower layer. The fluid flow induces a decrease of the pressure along the main channel while the static pressure in the detour channel remains constant and equal to the pressure value at the split point of the two channels. The increase of the applied pressure generates a larger pressure drop along the main channel and thus the pushup valve will progressively obstruct the main channel and generate a nonlinear fluidic behavior for Newtonian fluids (see Reference [40] for the characterization of the mechanical behavior of microfluidic valves in PDMS and Reference [41] for the flow-induced deformation of shallow microchannels in PDMS). Chang et al. proposed quantitative modeling of this microfluidic

system in PDMS used as a current source [39]. The  $Q(\Delta p)$  characteristic shows, at low pressure, a linear behavior with a slope inversely proportional to the hydraulic resistance of the non-deformed main channel. Further increasing the applied pressure gradient  $\Delta p$  induces nonlinearity due to the activation of the pushup valve, and the flow rate remains constant beyond a saturation pressure defined as the point where  $\frac{dQ(\Delta p)}{d\Delta p} = 0$ .

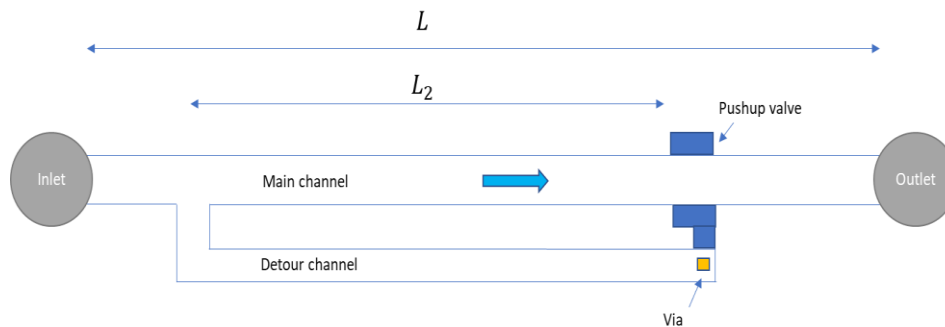


**Figure 7.** Schematic drawing of a microfluidic current source in PDMS comprising a main channel, a detour channel, and a pushup valve. The flow direction is indicated by the arrow (forward bias). The main and detour channel lengths are noted  $L$  and  $L_2$ , respectively. The increase of the inlet pressure generates a larger pressure drop along the main channel and thus the pushup valve will progressively obstruct the main channel and lead, beyond a saturation pressure, to a constant flow rate (adapted from Reference [39]).

Several microfluidic devices made of a stack of PDMS layers (Dow Corning Sylgard 184) with vertical connections (vias) were fabricated and tested using water. Constant flow rates of 0.015, 0.0198, and 0.024 mL/min were measured in the pressure range [620; 1240] mbar for detour channel ratio  $L_2/L$  of 0.8, 0.68, and 0.57 respectively, in good agreement with modeling data [37,39]. Liu et al. measured, for a fixed detour channel ratio of 0.66, the effect of the increase of the pushup valve width on saturation pressure and flow rate [38]. For pushup valve width of 100 and 110  $\mu\text{m}$ , the flow rate did not saturate, and the  $Q(\Delta p)$  showed a small and positive slope above 480 mbar. Saturation was obtained for pushup valve width of 120, 130, and 140  $\mu\text{m}$ , with saturation flow rate and pressure of 0.0027 mL/min in the range [350; 620] mbar, 0.0018 mL/min in the range [280; 620] mbar, and 0.0015 mL/min in the range [210; 620] mbar, respectively. As the valve width increases, the saturated flow rate and pressure decrease, as expected [39,40]. The authors reported that valves having widths of 150  $\mu\text{m}$  and more would irreversibly stick shut during either fabrication or operation [38]. The saturation point of this passive constant flow regulator for Newtonian fluids can thus be tuned by adjusting the detour channel ratio and the valve dimensions. These 3D structures in PDMS enable the miniaturization of autoregulatory devices for biochemical and biomedical applications.

#### Flow Regulator with Passive Membrane Valve in PDMS

Contrary to the detour autoregulators, the hydraulic resistance of the devices considered in this sub-section occurs mainly in the part of the main channel where the compliant valve is positioned. In 2009, Doh et al. developed a passive flow regulator in PDMS using parallel membrane valves [42]. A schematic cross-section of the device is shown in Figure 8. The increase  $\delta p$  of both inlet and sub-channel (or control channel) pressures induces a deflection of the two membranes. The narrowing of the fluid path leads to an increase  $\delta R_H$  of the main channel hydraulic resistance. Both analytical and 3D FEM simulations were carried out to design the passive constant flow regulators. The working principle is thus similar to the detour autoregulator made by Kartalov's group [37,39], except the fact that the pressure drop occurs here only in the space between the two thin membranes. The structure of the device is also simplified, and the minimum pressure to achieve flow regulation was lowered for better integration with micropumps.

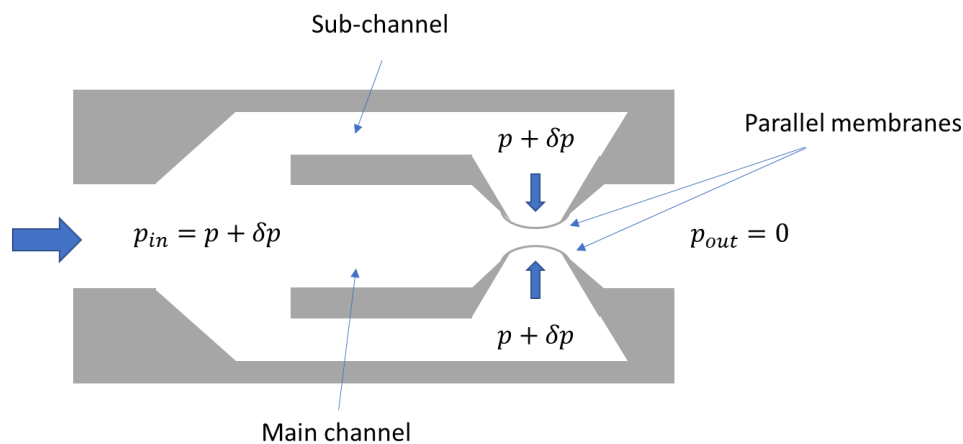


**Figure 8.** Schematic drawing of a passive flow regulator using autonomous deflection of parallel membrane valves. The increase  $\delta p$  of the inlet pressure induces a deflection of two membranes and thus an increase  $\delta R_h$  of the hydraulic resistance of the device (adapted from Reference [42]).

A single mask process was used to fabricate the device in PDMS, with SU-8 negative photoresist structure as a mold master. The microchannel height of the different prototypes is  $100\ \mu\text{m}$  and the main channel width is  $400\ \mu\text{m}$ . The  $100 \times 100\ \mu\text{m}$  thin square membranes are  $10\ \mu\text{m}$  thick. Four different prototypes having a width between the parallel membranes of 20, 30, 40, and  $50\ \mu\text{m}$  respectively, were tested with water. The  $20\ \mu\text{m}$  prototype fabricated by 10 : 1 PDMS (base/curing agent mixing ratio) and the  $40\ \mu\text{m}$  prototype fabricated by 20 : 1 PDMS showed a constant flow rate of  $0.3654\ \text{mL}/\text{min} \pm 3.8\%$  in the pressure range [200; 500] mbar and  $0.8718\ \text{mL}/\text{min} \pm 3.5\%$  in the pressure range [150; 500] mbar, respectively. The other prototypes, including the  $40\ \mu\text{m}$  prototype fabricated by 10:1 PDMS, did not show a constant flow rate. The prototypes made of 20 : 1 PDMS, which exhibits a lower Young's modulus than 10 : 1 PDMS, showed, as expected, a lower threshold pressure and a higher regulated flow rate than their counterparts made of 10:1 PDMS [42].

Zhang et al. further investigated this concept of passive flow regulators with elastomeric membranes and provided an analysis of the structural parameters that directly influence the flow rate [43–46]. Several passive flow regulators were built using standard soft lithography techniques [43,44], assembly of laser-structured thermoplastic films and PDMS membranes through roll-lamination method [45], or a combination of 3D printing and laser structuration/cutting [46]. PDMS, as a popular material for valve prototyping [47–49], was systematically used to form the thin membranes ( $10\ \mu\text{m}$  thick). Other layers are either made of PDMS [43,44], polyvinyl chloride (PVC) and polyethylene terephthalate (PET) [45], or photopolymer and silicon film [46]. The five-layer-stacked PDMS flow regulator comprises a bottom layer with a first control channel, a first membrane layer, a middle layer to form the main channel, a second membrane layer, and finally an upper layer with the second control channel and inlet and outlet ports [43,44]. The seven-layer-bond structure of the device made of PVC, PET, and PDMS comprises a base and a cover in PVC, and a fluidic layer in PVC between the upper and lower control layers in PET. Finally, the device made of photopolymer, a silicone film, and PDMS exhibits a four-layer structure with bottom and cover layers in photopolymer (structured using 3D printing technology), a seal layer in silicone, and the membrane in PDMS [46]. The working principle of this latter device, which furthermore comprises a check valve, is illustrated in Figure 9.

Zhang et al. manufactured and tested four different types of five-layer-stacked PDMS flow regulators noted (W200, L, H75) with different membrane lengths  $L$  (from 100 to  $400\ \mu\text{m}$ ) to study the influence of the flexible membrane length on the flow rate (see Table A1 in Appendix A) [43].  $W$  and  $H$  are respectively the width and the height of the contraction channel (i.e., valve) in  $\mu\text{m}$ , while  $L$  represents the width of the two aligned control channels (i.e., valve length). All flow-rate characteristics were measured using water. When the length of the membrane increases from 100 to  $400\ \mu\text{m}$ , the threshold

pressure and regulated flow rate decrease from 250 to 150 mbar and 2.55 to 1.12 mL/min, respectively. Six other PDMS flow regulators were characterized to study the influence of the cross-sectional dimensions on the flow rate: three samples (W100, L, H75) and three samples (W200, L, H130) with  $L = 200, 300, 400 \mu\text{m}$ , respectively. The measured regulated flow rates and threshold pressures are summarized in Table A1 in Appendix A. All results supported theoretical expectations: the stiffer the membrane, the higher the regulated flow rate and threshold pressure. As an example, increasing the height from  $75 \mu\text{m}$  (sample (W200, L400, H75)) to  $130 \mu\text{m}$  (sample (W200, L400, H130)) leads to a decrease of the threshold pressure from 150 to 100 mbar and an increase of the regulated flow rate from 1.12 to 2.79 mL/min [43]. Additional tests performed on a sample (W150, L300, H70) which exhibits, in static pressure conditions, a pressure threshold of 250 mbar and a regulated flow rate of  $1.49 \pm 0.018 \text{ mL/min}$ , showed that the autoregulation performances are maintained under sinusoidal varied pressures in the range [250;500] mbar [44]. Another version of this passive flow regulator with a seven-layer-bond architecture for improved manufacturing capabilities was characterized by Zhang et al. [45]. In the pressure range [200;700] mbar, the devices with channel heights of 90 and  $145 \mu\text{m}$  showed a regulated flow rate of respectively 1.36 and 0.29 mL/min. The four-layer structure made using 3D printing and UV laser cutting technologies was finally considered for prototyping a passive flow regulator, using a PDMS membrane of  $50 \mu\text{m}$  in thickness, an obstacle in the seal-layer of  $500 \times 800 \mu\text{m}$ , and channel height and width of respectively 250 and  $600 \mu\text{m}$ . The device, dedicated to low-cost and portable lab-on-a-chip (LOC) applications, showed a constant flow rate of  $25.2 \pm 1.2 \text{ mL/min}$  in the pressure range [700;1300] mbar.

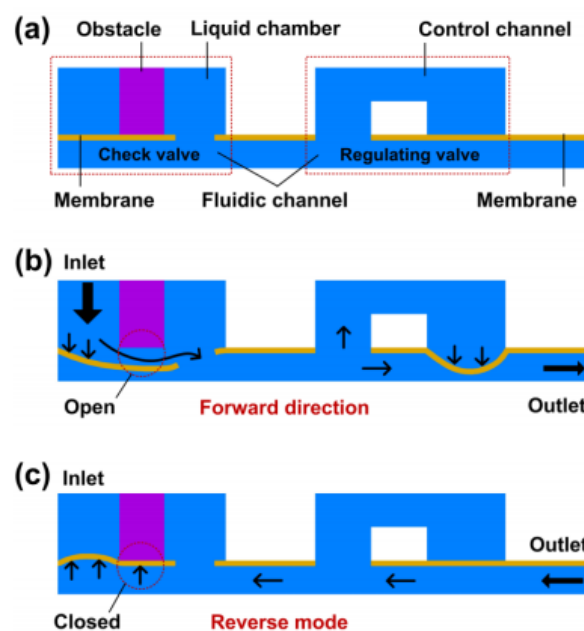


**Figure 9.** The working principle of the microfluidic device with a check valve and a flow regulating valve in PDMS. (a) Concept of the microchannel structure of the device at rest. (b) In the forward mode, the check valve is open and a flow regulating valve controls the liquid flowing through the microchannel. (c) In the reverse mode, the check valve is closed, and the flow is stopped (reprinted from Reference [46], Copyright MDPI).

#### Device with a Notched Pin and a Moving Elastomeric Membrane with a Central Through-Hole

The first mention of a flow-controlled hydrocephalus shunt was made, to the best of the author's knowledge, by Portnoy, who mentioned in 1982 that according to neurosurgeons' comments, the ideal valve should be flow-controlled such as to only remove the excess of cerebrospinal fluid (CSF) [50]. The first valve based on this principle, that the flow through the shunt shall not exceed the CSF production rate throughout the range of physiological intracranial pressures (ICP), was designed

by Sainte-rose et al. [51] and manufactured by Cordis Corporation. The valve labeled Orbis-Sigma<sup>®</sup> was first characterized in 1987 [51] and the later versions of this valve were included in many shunt evaluation campaigns (see, e.g., References [52–55]). A schematic drawing that illustrates the functioning principle of the valve is shown in Figure 10.

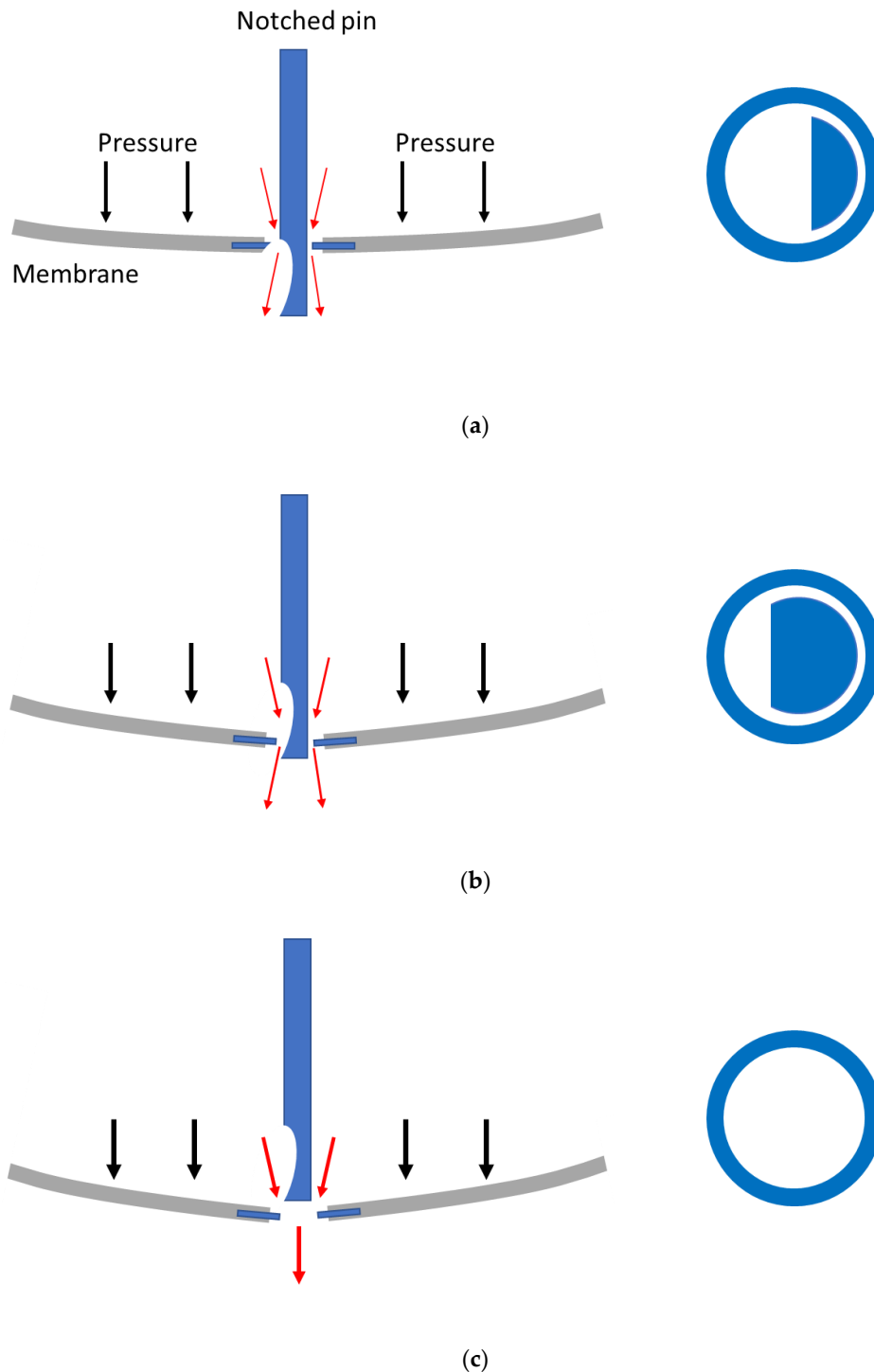


**Figure 10.** Schematic drawings of Orbis-Sigma II<sup>®</sup> valve (left) and cross-section of the orifice between the membrane and the pin (right). The cerebrospinal fluid (CSF) flow is indicated by an arrow. (a) Differential pressure stage, with a low hydraulic resistance up to 9 mbar. (b) Flow regulating stage, with a progressive narrowing of the orifice as the pressure increases from 9 to 36 mbar. (c) Safety stage beyond 36 mbar, with a low hydraulic resistance to restore normal ICP.

This passive flow-regulated valve has a flexible silicone membrane with a narrow orifice surrounding a pin of changing diameter. This three-stage valve has a fluidic characteristic similar to that of the passive high-flow regulator shown in Figure 2, with a regulated flow rate of about  $0.3 \text{ mL/min} \pm 15\%$  in the pressure range  $[9; 36] \text{ mbar}$  [55]. A low flow version (Integra NPH™) designed to meet the special needs of normal pressure hydrocephalus (NPH) patients requiring a lower flow rate of about  $0.2 \text{ mL/min}$ , throughout a similar pressure range, is also marketed by Integra LifeSciences [56]. In the first stage, also called the differential pressure stage, the valve operates similarly to standard differential pressure valves with low hydraulic resistance. At higher pressure, in the flow regulating stage, the membrane goes down and the pin progressively reduces the orifice to maintain the flow constant. The third stage of the valve, in high-pressure conditions (above 36 mbar), corresponds to the movement of the membrane beyond the pin. In this safety stage, the lowering of the hydraulic resistance enables a higher rate of CSF drainage to restore normal ICP.

### 3.2. Elastomeric Tubing with a Diamond-Shaped Aperture in the Sidewall

Another flow-controlled shunt design was disclosed by Paes in 1996 [8]. This CRx Diamond valve was manufactured by Phoenix Biomedical Corporation. The shunt mechanism, as illustrated in Figure 11, comprises a high-pressure relief valve (cruciform), an internal tube of an elastic wall forming the central channel with a diamond-shaped aperture in the sidewall, and a low-pressure outlet check valve (cruciform). As pressure increases, the tube contracts and narrows the side aperture. By design, the hydraulic resistance is expected to increase linearly with the pressure to regulate the flow. Beyond a predetermined threshold pressure, the high-pressure relief valve opens and the CSF flows through the wide central channel to restore normal ICP.

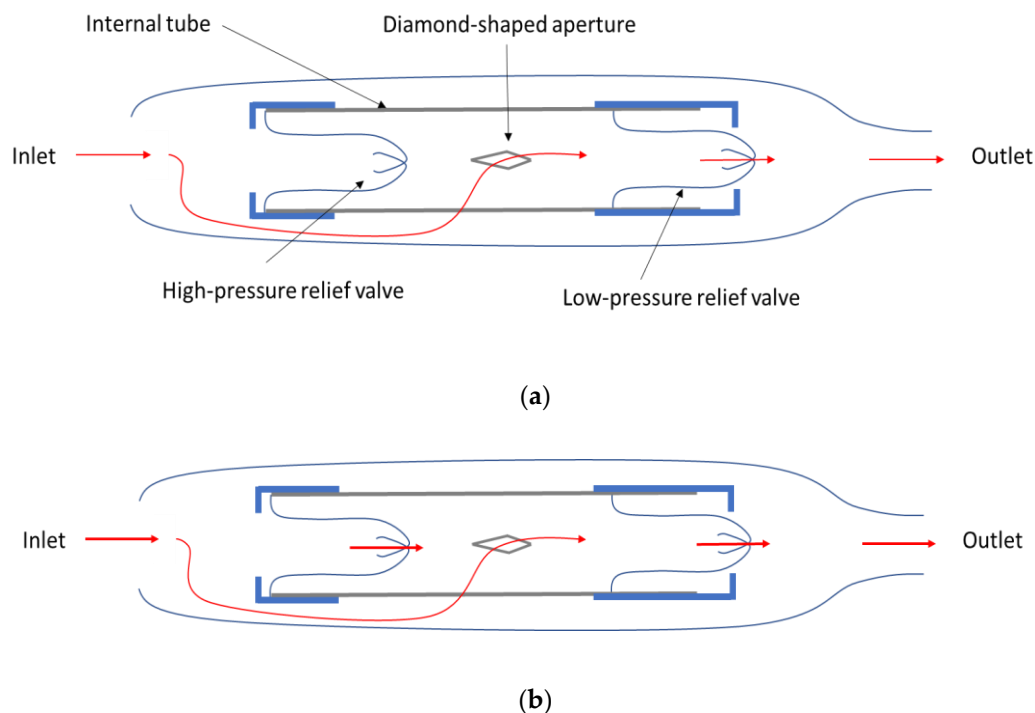


**Figure 11.** Schematic drawing of the CRx Diamond Valve, a flow control hydrocephalus shunt. The arrows indicate the flow direction. (a) Flow regulation stage, i.e., for pressure in the range  $[18.6; 30.6] \text{ mbar}$ . The CSF flows through the diamond-shaped aperture that narrows as the pressure increases to induce nonlinearity and through the low-pressure relief valve. (b) High-pressure or safety stage. The high-pressure relief valve opens to drain the excess of CSF through the large channel and the low-pressure relief valve.

Laboratory evaluation of the CRx Diamond Valve demonstrated a stabilized flow within the range 0.36 (for descending pressure) to 0.63 mL/min (for ascending pressure) when pressure varied in the range [18.6; 30.6] mbar. However, the stabilized flow decreased significantly over time, from 0.63 to 0.2 mL/min after 18 days. Czosnyka et al. also reported that the valve was insensitive to rapid fluctuations of differential pressure, small particles in the fluid, and reflux [57].

### 3.3. Spring Valve with a Spiral Groove on a Moving Piston

The design of the passive microfluidic devices described in the previous sections required two-dimensional (2D) or 3D FEM simulations of fluid flows fully coupled with structures undergoing large deformation, nonlinear material response, and contact conditions [58–63]. The non-well-defined Young's Modulus of some elastomeric materials (e.g., PDMS), coupled with the difficult adaptative meshing of high aspect ratio structures, are a challenge in computational engineering. The complexity is also due to the nonlinear change of the hydraulic resistance of the fluid path as its cross-section is varied. Amacker et al. [16] and Cousseau et al. [30] already considered a long channel with a fixed cross-section but the calculation of the spiral shape, to achieve a linear increase of the channel length as the pressure increases, is difficult due to notably the highly nonlinear deformation of the membrane after contact with the substrate [64].

A simpler design consists of a moving cylinder with a spiral groove and a linear compression spring inside a hollow cylinder with openings (see Figure 12). Due to the spring pretension, a minimum threshold pressure shall be applied at the inlet to move the piston that is initially partly engaged into the narrow part of the cylinder. As the pressure force on the piston increases, the piston is engaged further into the narrow part of the cylinder and the fluid is forced to flow through a longer channel length. If the linear spring is maintained within its nominal compression range, the counterforce generated by the spring increases linearly with the applied pressure. The induced movement of the piston leads to a linear increase of the channel length as the pressure increases, and since the channel cross-section and spiral pitch are constant, the flow is regulated at a predetermined fixed value. At high pressure, the piston movement is stopped, and the hydraulic resistance of the device can be either fixed (as illustrated in Figure 12), infinite (flow stopped) if the piston completely obstructs the fluid path, or very low (free flow) if openings are machined along the outlet port of the cylinder to by-pass the channel [7]. The pressure threshold that delimits the flow regulating stage of this valve can be modified by adjusting, for instance, the pretension or the length of the spring.

Such a device structure, which is very well suited for a high throughput application (up to 4 L/min or more), was also considered for hydrocephalus treatment [7]. A prototype in titanium was designed to drain CSF from the brain ventricles toward the peritoneal cavity. The piston has a diameter of 4 mm and the lathe tool with a tip curvature of 0.1 mm and an angle of 55° was used to form a 200 µm deep spiral groove with a pitch of 1.249 mm. The 10 mm custom-made spring used for the test exhibited a stiffness larger than expected (10 N/m instead of 8.3 N/m). The tests performed in a horizontal position using water at 20 °C showed, after extrapolation at 37 °C, a regulated flow rate of 0.35 mL/min ± 5% in the pressure range [10; 35] mbar. The spring stiffness offset induced a slight positive slope in the  $Q(\delta p)$  curve in good agreement with the theoretical expectations. In a vertical position, the gravitational force acts either in the same or opposite direction as the pressure forces onto the piston. To limit the effect of this induced pressure offset on the flow rate, a specific hollow piston that exhibits an overall density equal to water density has been machined. This gravity force on this piston in polyether ether ketone (PEEK) is balanced by Archimedes' force and the fluidic tests showed that the flow rate became insensitive to the device orientation.

The different parts of this passive constant flow regulating spring valve are compatible with standard machining techniques and can be characterized and sorted before the final assembly to improve the production yield. Given the impact of machining tolerances on flow rate accuracy, however, a minimum water flow rate of about 0.1 mL/min should be targeted.

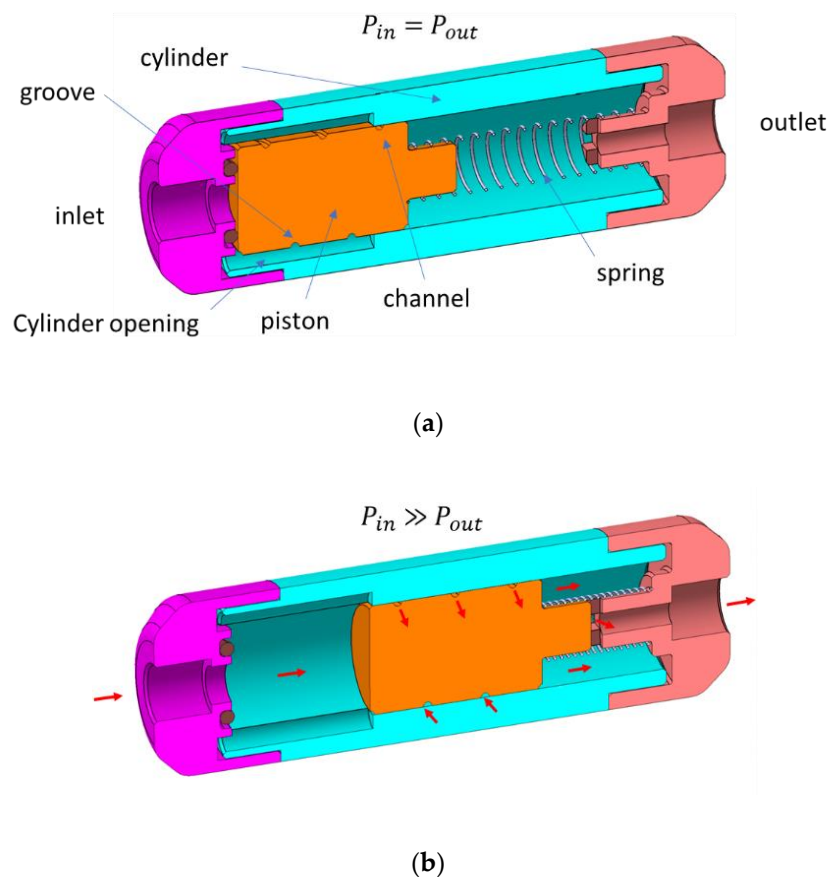


**Figure 12.** Schematic drawings of a constant flow regulating spring valve. (a) Device at rest. A small part of the piston groove is engaged into the narrow part of the cylinder to form a fluidic channel. (b) Device submitted to a large pressure  $P_{in} \gg P_{out}$ . As the inlet pressure increases, the piston moves along the cylinder and the channel length increases as well. At large pressure, the piston is stopped and the hydraulic resistance of the device becomes constant.

### 3.4. Device with a Thin Flexible Flap

The final category of passive flow control devices to be considered in this section refers to microfluidic devices comprising a thin flexible flap and stiff stopper that form a flow constriction in a microchannel. Yang et al. considered a planar flap/stopper configuration, as illustrated in Figure 13 [65]. The flap deflects towards the stopper with the applied pressure and narrows the fluid constriction. The resulting increase of the hydraulic resistance compensates for the pressure variations to maintain the forward flow rate constant. For reverse flow, the device exhibits a small hydraulic resistance and diodicity (the ratio of the backward pressure drop to the forward pressure drop [66]) up to  $10^5$  was measured experimentally [67].

This microfluidic variable resistor was fabricated in PDMS using standard replica molding techniques. The channel was formed by bonding the structured PDMS layer to flat PDMS or glass substrate(s) [65,67,68]. Yang et al. designed four different stopper/flap configurations: (a) basic design, as depicted in Figure 13, (b) centered stopper channel, (c) centered stopper channel with centered flap, and (d) double-flapped design [65]. All devices had a microchannel 300  $\mu\text{m}$  wide and 275  $\mu\text{m}$  high, a stopper channel 1000  $\mu\text{m}$  long and 40  $\mu\text{m}$  wide, and a flap-free end 33  $\mu\text{m}$  away from the channel sidewall. The designs a, b, c, and d have a flap 60, 50, 60, and 50  $\mu\text{m}$  wide and 36, 40, 45, and 50  $\mu\text{m}$  away from the stopper, respectively. Flow rate measurements were performed with water. Constant flow rates of 1.2, 0.16, 2.2, and 0.15 mL/min at  $\pm 3.5\%$  in the pressure range [1000;2000] mbar were measured for the designs a, b, c, and d, respectively [65]. Two other configurations designed using 3D fluid–structure interaction simulations were fabricated and tested later by Yang et al. [67,68],

the designs A and B with a flap 60 and 75  $\mu\text{m}$  wide and 36 and 25  $\mu\text{m}$  away from the stopper, respectively. Both designs had a microchannel 300  $\mu\text{m}$  wide and 275  $\mu\text{m}$  high, a flap 266  $\mu\text{m}$  wide and 275  $\mu\text{m}$  high, and a stopper channel 500  $\mu\text{m}$  long, 40  $\mu\text{m}$  wide, and 275  $\mu\text{m}$  high. The measured saturation threshold pressures are 900 mbar for design A and 600 mbar for design B. Constant flow rates of 0.21 and 1.2 mL/min at  $\pm 3\%$  at pressure up to 2000 mbar were reported for designs A and B, respectively.

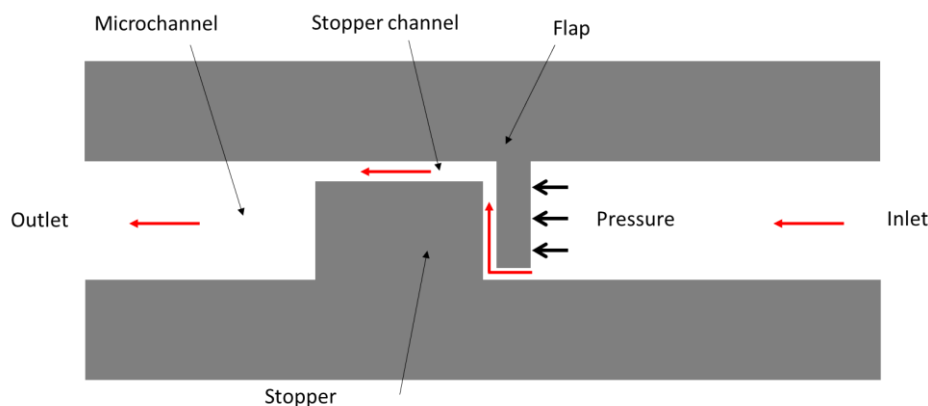


**Figure 13.** Schematic top view of a planar PDMS microfluidic flow regulator. The flow direction is indicated by red arrows. The flow restriction between the flap narrows with the applied pressure to maintain the flow rate constant.

Zhang et al. recently investigated a 3D-printed flap valve made of a photocurable resin [69]. The pressure-induced flap deflection narrows the flow restriction between the flap end and the microchannel sidewall. A theoretical model was developed to define the design rules. Using a flap with a tilt angle of  $40^\circ$ , a thickness of 300  $\mu\text{m}$ , and an initial gap of 300  $\mu\text{m}$ , Zhang et al. measured, with water, a large constant flow rate of 111 mL/min  $\pm 5.8\%$  in the pressure range [200;600] mbar.

#### 4. Non-Mechanical Passive Constant Flow Regulators

An original microfluidic passive flow regulator that can function at low  $Re$  without any moving parts was developed by Quake's group at Caltech in 2003 [13,70]. The nonlinearity required, as discussed in Section 2, for a passive constant flow regulator, derived from the non-Newtonian elastic properties of the working fluid, a 250 ppm by weight aqueous solution of a high molecular weight polyacrylamide. Two different designs of nonlinear channels were fabricated in PDMS using soft lithography [17,18]. The first channel is a chain of 46 identical halves of broad ellipsoidal rings (with inner half axes of 185 and 65  $\mu\text{m}$  and outer half axes of 410 and 290  $\mu\text{m}$ ) interconnected by a narrow bottleneck ( $\approx 30 \mu\text{m}$ ), while the second channel is a chain of 43 identical triangular segments (about 203 by 330  $\mu\text{m}$ ) interconnected by a bottleneck contraction of about 37  $\mu\text{m}$ . The viscoelastic solution is therefore forced to flow through a sequence of expansions and contractions. The polymer molecules become extended along the flow direction when the working fluid flows through a contraction. If the extension rate is large enough compared to  $1/\lambda$  (where  $\lambda$  is the relaxation time of the polymer solution), the molecules can unravel and generate nonlinearity with an increase of the apparent viscosity of the solution [71]. Both devices behave as a three-stage valve with two inflection points in the  $Q(\Delta p)$  characteristics. The first device showed a linear increase in the flow rate with the pressure until a transition when the flow rate reaches 15 nL/s. Constant flow rates of  $18.7 \pm 0.6$  nL/s for a  $\Delta p$  per segment in the range [0.5;1] mbar and  $20 \pm 5$  nL/s for a  $\Delta p$  per segment in the range [0.22;2.2] mbar are reported [13]. At higher pressure, the differential flow resistance  $dP/dQ$  decreases. The second device exhibited a flow transition at 17 nL/s but the nonlinear increase of the resistance did not yield a flow stabilization when the pressure gradient per segment became larger than 0.07 mbar [70]. At low  $Re$  ( $\ll 1$ ), the Navier-Stokes equations become linear and flow is expected to be completely reversible [72]. Therefore, the channel

shall exhibit the same hydraulic resistance for both flow directions. Groisman demonstrated with the second device a diodicity of about 2, which was a signature, in absence of significant inertial effects, of a flow rectification due to nonlinear elastic properties of the working fluid [70]. Such devices may be integrated into a drug delivery system if a biocompatible polymer solution is used.

## 5. Conclusions

Active fluid control poses numerous problems of integration and miniaturization, and the development of microvalves and micropumps, which are two important building blocks of a microfluidic platform, was stimulated by recent advances in lab-on-a-chip for diagnostics applications, drug delivery, flow chemistry, point-of-care testing, etc. Compared to active microvalves [73], passive constant flow control valves provide a simpler way to regulate fluid flows without external control and energy consumption. This review has examined the wide variety of passive flow regulators that have been developed over the last 30 years. The modeling, the fabrication methods, and the resulting performance of these passive microvalves have been constantly improved. Table 2 summarized the principal pros and cons of each category of passive flow regulators.

Hysteresis was not included in this comparative table because this effect should be better characterized. Besides, considerations relative to the manufacturing reproducibility of the passive flow regulators made in PDMS are still speculative and have yet to be demonstrated. Recent advances in the development of these devices are promising but Table 2 also suggests that there is still room for further developing the technology and designing passive constant flow regulators that ideally combine the reliability and performance of MEMS-based valves with the ease of production and the large integration capability of their PDMS counterparts.

**Table 2.** Comparative table of the different categories of passive constant flow regulators.

	Pressure Range	Flow Rate Range	Accuracy/Reproducibility	Connectivity	Fabrication Cost	Prototyping Complexity	Aqueous Solution
<b>MECHANICAL</b>							
Si membrane(s)	Very large	Very large	High/Very High	Medium	Low */High	High	Yes
Elastomeric membrane(s)	Large	Very large	High/Medium **	High	Low/Medium	Low/Medium	Yes
Tube with lateral aperture	Small	Small	Low/Low	Medium	Low	Low	Yes
Piston	Large	Large	High/Medium **	Medium	Medium	Medium	Yes
Flap	Large	Large	High/Medium **	High	Low/Medium	Low/Medium	Yes
<b>NON-MECHANICAL</b>							
Rheological	Small	Small	Low/Medium **	High	Low	Low	No

\* At large volumes only; \*\* Estimation.

**Funding:** This research received no external funding.

**Acknowledgments:** The author would like to thank Dimitry Dumont-fillon for proof-reading the manuscript.

**Conflicts of Interest:** The author declares no conflict of interest.

## Nomenclature

Symbol	Name	Units
H	Height	m
L	Length	m
$p$	Pressure	Pa
$P_{in}, P_{out}$	Inlet/Outlet pressure	Pa
$\Delta p$	Pressure gradient	Pa
$\Delta P_{reg\ min}, \Delta P_{reg\ max}$	Minimum/Maximum pressure gradient to achieve the nominal flow rate	Pa
$\Delta P_{off}$	Shut-off pressure gradient	Pa
$Q, Q_0$	Flow rate, Nominal flow rate	$m^3 \cdot s^{-1}$
$R_h$	Hydrodynamic resistance	$Pa \cdot s \cdot m^{-3}$
T	Temperature	K
v	Velocity	$m \cdot s^{-1}$
W	Width	m
$\eta$	Dynamic viscosity	Pa·s
$\lambda$	Relaxation time of a polymer solution	s
Re	Reynolds number	-
Kn	Knudsen number	-
Abbreviation	Name	
BioMEMS	Biomedical microelectromechanical system	
CSF	Cerebrospinal fluid	
CTQ	Critical-to-quality	
EOF	Electroosmotic flow	
FEM	Finite element method	
FSI	Fluid–structure interaction	
HF	Hydrofluoric acid	
ICP	Intracranial Pressure	
KOH	Potassium hydroxide	
LOC	Lab-on-a-chip	
MEMS	Microelectromechanical system	
NPH	Normal-pressure hydrocephalus	
PDMS	Poly(dimethylsiloxane)	
PE	Polyethylene	
PET	Polyethylene terephthalate	
PEEK	Polyether ether ketone	
PVC	Polyvinyl chloride	
Si	Silicon	
SOI	Silicon on insulator	
Ti	Titanium	
$\mu$ TAS	Micro total analysis system	

Appendix A

Table A1. Passive constant flow regulators.

Author and Year	Name/Description	Construction	Working Fluid	Plateau Pressure (mbar)		Flow Rate (mL/min)	SD (%)
				Min	Max		
<b>MECHANICAL PASSIVE CONSTANT FLOW REGULATORS</b>							
<b>Devices with Flexible Silicon Membrane(s)</b>							
Park 1988 [29]	Micromachined passive flow regulator	Rectangular Si membrane ( $h_{\text{channel}} 9.5 \mu\text{m}$ , $t_{\text{memb}} 26 \mu\text{m}$ , $L/W = 2$ )	Water	200	400	0.0150	n/r
Amacker 1998 [16]	Micromachined passive flow regulator	Membrane + spiral-shaped channel in Si/Pyrex or Titanium	Water	100	600	0.0003	10.00
Cousseau 2001 [30]	Passive flow regulator	Si membrane + spiral channel in Si substrate	Water	180	500	0.0142	5.0
Chappel 2014 [33]	Passive flow regulator	Drilled Si membrane + pillar substrate in Pyrex	Water	50	150	0.225	n/r
Cornaggia 2017 [22]	Passive flow regulator	Drilled Si membrane + pillar substrate in Pyrex (design A)	Water + Glycerol/12cP	4000	21,000	0.6	5.0
		Drilled Si membrane + pillar substrate in Pyrex (design B)	Water + Glycerol/24cP	8000	21,000	0.5	5.0
		Drilled Si membrane + pillar substrate in Pyrex (design C)	Water + Glycerol/24cP	7000	21,000	0.13	5.0
Conti 2018 [34]	Passive flow regulator	Drilled Si membrane + Si pillar substrate (design 1 mL/min at 12cP)	Water + Glycerol/12cP	8000	19,000	0.95	5.0
		Drilled Si membrane + Si pillar substrate (design 0.2 mL/min at 24cP)	Water + Glycerol/24cP	6000	19,000	0.21	5.0
Dumont-fillon 2020 [9]	Passive flow regulator	3-stack MEMS based device in Si and glass (1 mL/day design)	Water	200	800	0.000694	10.0
		3-stack MEMS based device in Si and glass (1 mL/h design)	Water	200	800	0.0167	10.0
<b>Devices with Compliant Elastomeric Membrane(s)</b>							
Kartalov 2006 [37], Chang 2012 [39]	Detour autoregulator	PDMS channel + pushup valve ( $L_2/L = 0.8$ )	Water	620	1240	0.015	n/r

Table A1. Cont.

Author and Year	Name/Description	Construction	Working Fluid	Plateau Pressure (mbar)		Flow Rate (mL/min)	SD (%)
				Min	Max		
<b>MECHANICAL PASSIVE CONSTANT FLOW REGULATORS</b>							
		PDMS channel + pushup valve ( $L_2/L = 0.68$ )	Water	620	1240	0.0198	n/r
		PDMS channel + pushup valve ( $L_2/L = 0.57$ )	Water	620	1240	0.0240	n/r
Liu 2009 [38]	Detour autoregulator	PDMS channel + pushup valve ( $L_2/L = 0.66$ , width 120 $\mu\text{m}$ )	Water	350	620	0.0027	n/r
		PDMS channel + pushup valve ( $L_2/L = 0.66$ , width 130 $\mu\text{m}$ )	Water	280	620	0.0018	n/r
		PDMS channel + pushup valve ( $L_2/L = 0.66$ , width 140 $\mu\text{m}$ )	Water	210	620	0.0015	n/r
Doh 2009 [42]	Parallel membrane valve	Thin PDMS membrane—width of 20 $\mu\text{m}$	Water	200	500	0.3654	3.8 *
		Thin PDMS membrane—width of 40 $\mu\text{m}$	Water	150	500	0.8718	3.5 *
Zhang 2015 [43]	Passive flow regulator	Five-layer-stacked PDMS device—membrane (W200, L100, H75) in $\mu\text{m}$	Water	250	500	2.55	2.4 *
		Five-layer-stacked PDMS device—membrane (W200, L200, H75) in $\mu\text{m}$	Water	250	500	2.06	3.9 *
		Five-layer-stacked PDMS device—membrane (W200, L300, H75) in $\mu\text{m}$	Water	200	500	1.41	4.3 *
		Five-layer-stacked PDMS device—membrane (W200, L400, H75) in $\mu\text{m}$	Water	150	500	1.12	4.5 *
		Five-layer-stacked PDMS device—membrane (W100, L200, H75) in $\mu\text{m}$	Water	200	500	1.09	4.6 *
		Five-layer-stacked PDMS device—membrane (W100, L300, H75) in $\mu\text{m}$	Water	200	500	0.92	4.4 *
		Five-layer-stacked PDMS device—membrane (W100, L400, H75) in $\mu\text{m}$	Water	150	500	0.86	4.7 *
		Five-layer-stacked PDMS device—membrane (W200, L200, H130) in $\mu\text{m}$	Water	150	500	4.38	2.3 *

Table A1. Cont.

Author and Year	Name/Description	Construction	Working Fluid	Plateau Pressure (mbar)		Flow Rate (mL/min)	SD (%)
				Min	Max		
<b>MECHANICAL PASSIVE CONSTANT FLOW REGULATORS</b>							
		Five-layer-stacked PDMS device—membrane (W200, L300, H130) in $\mu\text{m}$	Water	150	500	4.92	4.9 *
		Five-layer-stacked PDMS device—membrane (W200, L400, H130) in $\mu\text{m}$	Water	100	500	2.79	4.7 *
Zhang 2016 [44]	Passive flow regulator	Five-layer-stacked PDMS device—membrane (W150, L300, H70) in $\mu\text{m}$	Water	250	500	1.49	1.2 *
Zhang 2017 [45]	Microfluidic autoregulatory valve (channel height 145 $\mu\text{m}$ )	Seven-layer-bond structure (polymer films and PDMS membranes)	Water	200	700	1.36	3.4 *
	Microfluidic autoregulatory valve (channel height 90 $\mu\text{m}$ )	Seven-layer-bond structure (polymer films and PDMS membranes)	Water	200	700	0.29	4.2 *
Zhang 2019 [46]	Passive flow regulator with check valve in reverse mode	Four-layer structure with thin PDMS membrane and silicone film	Water	700	1300	25.2	5 *
Chari 2014 [55]	CSF shunt/Integra OSV II (Integra LifeScience)—normal flow	Moving elastomeric membrane + notched pin	Water (test)/CSF	9	36	0.3	15.0
Codman 2018 [56]	CSF shunt/Integra NPH (Integra LifeScience)—low flow	Moving elastomeric membrane + notched pin	Water (test)/CSF	12	30	0.2	n/r
<b>Elastomeric Tubing with a Diamond-Shaped Aperture in the Sidewall</b>							
Paes 1996 [8], Czosnyka 2001 [57]	CSF shunt/CRx Diamond Valve (Phoenix Biomedical Corp.)	Elastomeric tube with a longitudinal aperture in the side wall	Water (test)/CSF	18.6	30.6	0.63 (ascending pressure)	50.0
		Elastomeric tube with a longitudinal aperture in the side wall	Water (test)/CSF	18.6	30.6	0.36 (descending pressure)	22.0

Table A1. Cont.

Author and Year	Name/Description	Construction	Working Fluid	Plateau Pressure (mbar)		Flow Rate (mL/min)	SD (%)
				Min	Max		
<b>MECHANICAL PASSIVE CONSTANT FLOW REGULATORS</b>							
<b>Spring Valve with a Spiral Groove on a Moving Piston</b>							
Chappel 2016 [7]	CSF shunt/flow regulator	Titanium/PEEK spring valve with spiral groove on a moving cylinder	Water (test)/CSF	10	35	0.35	5 *
<b>Device with a Thin Flexible Flap</b>							
Yang 2004 [65]	Passive flow regulator in PDMS	PDMS flap + Stopper (design a: flap 60 $\mu$ m; d(flap-stopper) = 36 $\mu$ m)	Water	1000	2000	1.2	3.5 *
		PDMS flap + Stopper (design b: flap 50 $\mu$ m; d(flap-stopper) = 40 $\mu$ m)	Water	1000	2000	0.16	3.5 *
		PDMS flap + Stopper (design c: flap 60 $\mu$ m; d(flap-stopper) = 45 $\mu$ m)	Water	1000	2000	2.2	3.5 *
		PDMS flap + Stopper (design d: flap 50 $\mu$ m; d(flap-stopper) = 50 $\mu$ m)	Water	1000	2000	0.15	3.5 *
Yang 2007 [67], Yang 2007 [68]	Passive flow regulator in PDMS	PDMS flap + Stopper (design A: flap 60 $\mu$ m; d(flap-stopper) = 36 $\mu$ m)	Water	600	2000	0.21	3.0 *
		PDMS flap + Stopper (design B–flap 75 $\mu$ m; d(flap-stopper) = 25 $\mu$ m)	Water	900	2000	1.2	3.0 *
Zhang 2020 [69]	Self-adaptative flexible valve as passive flow regulator	Flap (cantilever) in a channel	Water	200	600	111	5.8 *
<b>NON-MECHANICAL PASSIVE CONSTANT FLOW REGULATORS</b>							
<b>Rheological</b>							
Groisman 2003 [13]	Non-linear resistor/Rheological	PDMS microchannels	Viscoelastic polymer solution	10	100	0.0012	25.0

n/r: not reported; L2/L: detour channel ratio; \* deviation to linearity measured on a single sample.

## References

1. Warring, R.H. *Hydraulic Handbook*; Gulf Publishing Company: Houston, TX, USA, 1983; pp. 117–119.
2. Cundiff, J.S. *Fluid Power Circuits and Controls: Fundamentals and Applications*; CRC Press: Boca Raton, FL, USA, 2001; pp. 140–143.
3. Laser, D.J.; Santiago, J.G. A review of micropumps. *J. Micromech. Microeng.* **2004**, *14*, R35–R64. [[CrossRef](#)]
4. Whitesides, G.M. The origins and the future of microfluidics. *Nature* **2006**, *442*, 368–373. [[CrossRef](#)] [[PubMed](#)]
5. White, F.M. *Viscous Fluid Flow*, 2nd ed.; McGraw-Hill: New York, NY, USA, 1991.
6. Chappel, E. (Ed.) *Drug Delivery Devices and Therapeutic Systems*; Academic Press: New York, NY, USA, 2020.
7. Chappel, E. Design and characterization of a passive flow control valve dedicated to the hydrocephalus treatment. *Cogent Eng.* **2016**, *3*, 1247612. [[CrossRef](#)]
8. Paes, N.A. New self-adjusting flow-regulating device for shunting of CSF. *Childs Nerv. Syst.* **1996**, *12*, 619–625. [[CrossRef](#)] [[PubMed](#)]
9. Dumont-Fillon, D.; Lamaison, D.; Chappel, E. Design and characterization of 3-stack MEMS-based passive flow regulators for implantable and ambulatory infusion pumps. *J. Microelectromech. Syst.* **2020**, *29*, 170–181. [[CrossRef](#)]
10. Skryabina, E.A.; Dunn, T.S. Disposable infusion pumps. *Am. J. Health-Syst. Pharm.* **2006**, *63*, 1260–1268. [[CrossRef](#)]
11. Capes, D.F.; Asimwe, D. Performance of selected flow-restricting infusion devices. *Am. J. Health Syst. Pharm.* **1998**, *55*, 351–359. [[CrossRef](#)]
12. Ilfeld, B.M.; Morey, T.E.; Enneking, F.K. The delivery rate accuracy of portable infusion pumps used for continuous regional analgesia. *Anesth. Analg.* **2002**, *95*, 1331–1336. [[CrossRef](#)]
13. Groisman, A.; Enzelberger, M.; Quake, S.R. Microfluidic memory and control devices. *Science* **2003**, *300*, 955–958. [[CrossRef](#)]
14. Roy, S.; Raju, R.; Chuang, H.F.; Cruden, B.A.; Meyyappan, M. Modeling gas flow through microchannels and nanopores. *J. Appl. Phys.* **2003**, *93*, 4870–4879. [[CrossRef](#)]
15. Kestin, J.; Sokolov, M.; Wakeham, W.A. Viscosity of liquid water in the range  $-8\text{ }^{\circ}\text{C}$  to  $150\text{ }^{\circ}\text{C}$ . *J. Phys. Chem. Ref. Data* **1978**, *7*, 941–948. [[CrossRef](#)]
16. Amacker, C.; Leung Ki, Y.-S.; Pasquier, V.; Madore, C.; Haller, M.; Renaud, P.; White, N. Passive micro-flow regulator for drug delivery system. In Proceedings of the Eurosensors XII Conference, Southampton, UK, 13–16 September 1998; pp. 591–594.
17. Duffy, D.C.; McDonald, J.C.; Schueller, O.J.; Whitesides, G.M. Rapid prototyping of microfluidic systems in poly (dimethylsiloxane). *Anal. Chem.* **1998**, *70*, 4974–4984. [[CrossRef](#)] [[PubMed](#)]
18. McDonald, J.C.; Duffy, D.C.; Anderson, J.R.; Chiu, D.T.; Wu, H.; Schueller, O.J.; Whitesides, G.M. Fabrication of microfluidic systems in poly (dimethylsiloxane). *Electrophoresis* **2000**, *21*, 27–40. [[CrossRef](#)]
19. Sackmann, E.K.; Fulton, A.L.; Beebe, D.J. The present and future role of microfluidics in biomedical research. *Nature* **2014**, *507*, 181–189. [[CrossRef](#)]
20. Quake, S.R.; Scherer, A. From micro-to nanofabrication with soft materials. *Science* **2000**, *290*, 1536–1540. [[CrossRef](#)]
21. Petersen, K.E. Silicon as a mechanical material. *Proc. IEEE* **1982**, *70*, 420–457. [[CrossRef](#)]
22. Cornaggia, L.; Conti, L.; Hannebelle, M.; Gamper, S.; Dumont-Fillon, D.; Van Lintel, H.; Renaud, P.; Chappel, E. Passive flow control valve for protein delivery. *Cogent Eng.* **2017**, *4*, 1413923. [[CrossRef](#)]
23. Oseyemi, A.E.; Zhang, X. Theoretical modeling of the behavior of a parallel membrane passive flow regulator. *Sens. Actuator A Phys.* **2020**, *315*, 112310. [[CrossRef](#)]
24. Dumont-Fillon, D.; Hannebelle, M.; Van Lintel, H.; Chappel, E. Design of a passive flow regulator using a genetic algorithm. *Procedia Eng.* **2016**, *168*, 1016–1019. [[CrossRef](#)]
25. Zengerle, R.; Richter, M. Simulation of microfluid systems. *J. Micromech. Microeng.* **1994**, *4*, 192–204. [[CrossRef](#)]
26. Bourouina, T.; Grandchamp, J.-P. Modeling micropumps with electrical equivalent networks. *J. Micromech. Microeng.* **1996**, *6*, 398–404. [[CrossRef](#)]
27. Chappel, E.; Hannebelle, M.; Cornaggia, L.; Dumont-Fillon, D.; Momjian, S. Hybrid hydrodynamic characteristic for hydrocephalus valve: A numerical investigation using electrical equivalent networks. *Cogent Eng.* **2017**, *4*, 1415103. [[CrossRef](#)]

28. Tachatos, N.; Chappel, E.; Dumont-Fillon, D.; Meboldt, M.; Daners, M.S. Posture related in-vitro characterization of a flow regulated MEMS CSF valve. *Biomed. Microdevices* **2020**, *22*, 1–12. [[CrossRef](#)]
29. Park, S.; Ko, W.; Prael, J. A Constant flow-rate microvalve actuator based on silicon and micromachining technology. In Proceedings of the IEEE Technical Digest on Solid-State Sensor and Actuator Workshop, Hilton Head Island, SC, USA, 6–9 June 1988; pp. 136–139.
30. Cousseau, P.; Hirschi, R.; Frehner, B.; Gamper, S.; Maillefer, D. Improved micro-flow regulator for drug delivery systems. In Proceedings of the 14th IEEE International Conference on Micro Electro Mechanical Systems MEMS 2001, Interlaken, Switzerland, 21–25 January 2001; pp. 527–530.
31. Chappel, E. Passive Fluid Flow Regulator. U.S. Patent US8539981 (B2), 24 September 2013.
32. Chappel, E.; Musard, H.; Dumont-fillon, D. Experimental characterization and modelling of microfluidic radial diffusers for passive self-regulating valves. *Glob. J. Eng. Tech. Adv.* **2019**, *1*, 10–21. [[CrossRef](#)]
33. Chappel, E.; Dumont-Fillon, D.; Mefti, S. Passive flow regulators for drug delivery and hydrocephalus treatment. In Proceedings of the Microfluidics, BioMEMS, and Medical Microsystems XII Conference (International Society for Optics and Photonics), San Francisco, CA, USA, 2–4 February 2014; Volume 8976, p. 89760S.
34. Conti, L.; Dumont-Fillon, D.; van Lintel, H.; Chappel, E. Silicon-to-silicon anodic bonding via intermediate borosilicate layer for passive flow control valves. *Int. J. Mech. Ind. Aero. Sci.* **2018**, *12*, 701–704.
35. Chappel, E. Adjustable Passive Flow Regulator. European Patent EP2943708B1, 6 September 2017.
36. Yang, B.; Metier, J.L.; Lin, Q. Using compliant membranes for dynamic flow stabilization in microfluidic systems. In Proceedings of the 18th IEEE International Conference on Micro Electro Mechanical Systems MEMS 2005, Miami Beach, FL, USA, 30 January–3 February 2005; pp. 706–709.
37. Kartalov, E.P.; Walker, C.; Taylor, C.R.; Anderson, W.F.; Scherer, A. Microfluidic vias enable nested bioarrays and autoregulatory devices in newtonian fluids. *Proc. Natl. Acad. Sci. USA* **2006**, *103*, 12280–12284. [[CrossRef](#)] [[PubMed](#)]
38. Liu, J.; Chen, Y.; Taylor, C.R.; Scherer, A.; Kartalov, E.P. Elastomeric microfluidic diode and rectifier work with newtonian fluids. *J. Appl. Phys.* **2009**, *106*, 114311. [[CrossRef](#)]
39. Chang, H.-J.; Ye, W.; Kartalov, E.P. Quantitative modeling of the behaviour of microfluidic autoregulatory devices. *Lab. Chip* **2012**, *12*, 1890–1896. [[CrossRef](#)]
40. Kartalov, E.P.; Scherer, A.; Quake, S.R.; Taylor, C.R.; Anderson, W.F. Experimentally validated quantitative linear model for the device physics of elastomeric microfluidic valves. *J. Appl. Phys.* **2007**, *101*, 064505. [[CrossRef](#)]
41. Gervais, T.; El-Ali, J.; Günther, A.; Jensen, K.F. Flow-induced deformation of shallow microfluidic channels. *Lab. Chip* **2006**, *6*, 500–507. [[CrossRef](#)]
42. Doh, I.; Cho, Y.H. Passive flow-rate regulators using pressure-dependent autonomous deflection of parallel membrane valves. *Lab. Chip* **2009**, *9*, 2070–2075. [[CrossRef](#)] [[PubMed](#)]
43. Zhang, X.; Xiang, N.; Tang, W.; Huang, D.; Wang, X.; Yi, H.; Ni, Z. A passive flow regulator with low threshold pressure for high-throughput inertial isolation of microbeads. *Lab. Chip* **2015**, *15*, 3473–3480. [[CrossRef](#)] [[PubMed](#)]
44. Zhang, X.; Wang, X.; Chen, K.; Cheng, J.; Xiang, N.; Ni, Z. Passive flow regulator for precise high-throughput flow rate control in microfluidic environments. *RSC Adv.* **2016**, *6*, 31639–31646. [[CrossRef](#)]
45. Zhang, X.; Zhu, Z.; Ni, Z.; Xiang, N.; Yi, H. Inexpensive, rapid fabrication of polymer-film microfluidic autoregulatory valve for disposable microfluidics. *Biomed. Microdevices* **2017**, *19*, 21. [[CrossRef](#)] [[PubMed](#)]
46. Zhang, X.; Zhang, Z. Microfluidic passive flow regulatory device with an integrated check valve for enhanced flow control. *Micromachines* **2019**, *10*, 653. [[CrossRef](#)] [[PubMed](#)]
47. Kawai, K.; Arima, K.; Morita, M.; Shoji, S. Microfluidic valve array control system integrating a fluid demultiplexer circuit. *J. Micromech. Microeng.* **2015**, *25*, 065016. [[CrossRef](#)]
48. Hansson, J.; Hillmering, M.; Haraldsson, T.; van der Wijngaart, W. Leak-tight vertical membrane microvalves. *Lab. Chip* **2016**, *16*, 1439–1446. [[CrossRef](#)]
49. Rho, H.S.; Yang, Y.; Hanke, A.T.; Ottens, M.; Terstappen, L.W.; Gardeniers, H. Programmable V-type valve for cell and particle manipulation in microfluidic devices. *Lab. Chip* **2016**, *16*, 305–311. [[CrossRef](#)]

50. Portnoy, H.D. Hydrodynamics of shunts. *Monogr. Neural Sci.* **1982**, *8*, 179–183.
51. Sainte-Rose, C.; Hooven, M.D.; Hirsch, J.-F. A New approach in the treatment of hydrocephalus. *J. Neurosurg.* **1987**, *66*, 213–226. [[CrossRef](#)]
52. Drake, J.M.; Kestle, J. Rationale and methodology of the multicenter pediatric cerebrospinal fluid shunt design trial. *Child's Nerv. Syst.* **1996**, *12*, 434–447. [[CrossRef](#)] [[PubMed](#)]
53. Drake, J.M.; Kestle, J.R.; Milner, R.; Cinalli, G.; Boop, F.; Piatt, J.; Haines, S.; Schiff, S.J.; Cochrane, D.D.; Steinbok, P. Randomized trial of cerebrospinal fluid shunt valve design in pediatric hydrocephalus. *Neurosurgery* **1998**, *43*, 294–303. [[CrossRef](#)]
54. Hanlo, P.W.; Cinalli, G.; Vandertop, W.P.; Faber, J.A.; Bøgeskov, L.; Børgesen, S.E.; Boschert, J.; Chumas, P.; Eder, H.; Pople, I.K. Treatment of hydrocephalus determined by the european orbis sigma valve II survey: A multicenter prospective 5-year shunt survival study in children and adults in whom a flow-regulating shunt was used. *J. Neurosurg.* **2003**, *99*, 52–57. [[CrossRef](#)] [[PubMed](#)]
55. Chari, A.; Czosnyka, M.; Richards, H.K.; Pickard, J.D.; Czosnyka, Z.H. Hydrocephalus shunt technology: 20 years of experience from the Cambridge shunt evaluation laboratory. *J. Neurosurg.* **2014**, *120*, 697–707. [[CrossRef](#)] [[PubMed](#)]
56. Codman specialty surgical. In *Flow Regulating Valves*; Integra LifeSciences Corporation: Princeton, NJ, USA, 2018.
57. Czosnyka, Z.H.; Czosnyka, M.; Richards, H.K.; Pickard, J.D. Laboratory evaluation of the Phoenix CRx diamond valve. *Neurosurg.* **2001**, *48*, 689–694. [[CrossRef](#)] [[PubMed](#)]
58. Senturia, S.D. CAD Challenges for microsensors, microactuators, and microsystems. *Proc. IEEE* **1998**, *86*, 1611–1626. [[CrossRef](#)]
59. Oosterbroek, R.; Berenschot, J.W.; Schlautmann, S.; Lammerink, T.S.; van den Berg, A.; Elwenspoek, M.C. Modeling and validation of fluid structure interactions in passive micro valves. In Proceedings of the 1998 International Conference on modelling and Simulation of Microsystems Semiconductors, Santa Clara, CA, USA, 6–8 April 1998; pp. 528–533.
60. Dowell, E.H.; Hall, K.C. Modeling of fluid-structure interaction. *Annu. Rev. Fluid Mech.* **2001**, *33*, 445–490. [[CrossRef](#)]
61. Smal, O.; Raucant, B.; Jeanmart, H. Fluid flow modelling of a micro-valve. *Int. J. Simul. Multidiscip. Des. Optim.* **2009**, *3*, 356–362. [[CrossRef](#)]
62. Chakraborty, D.; Prakash, J.R.; Friend, J.; Yeo, L. Fluid-structure interaction in deformable microchannels. *Physics Fluids* **2012**, *24*, 102002. [[CrossRef](#)]
63. Lin, Z.-H.; Li, X.-J.; Jin, Z.-J.; Qian, J.-Y. Fluid-structure interaction analysis on membrane behavior of a microfluidic passive valve. *Membranes* **2020**, *10*, 300. [[CrossRef](#)]
64. Timoshenko, S.P.; Woinowsky-Krieger, S. *Theory of Plates and Shells*, 2nd ed.; McGraw-Hill: New York, NY, USA, 1959; pp. 308–310.
65. Yang, B.; Levis, J.W.; Lin, Q. A PDMS-based constant-flowrate microfluidic control device. In Proceedings of the 17th IEEE International Conference MEMS 2004, Maastricht, The Netherlands, 25–29 January 2004; pp. 379–382.
66. Fadl, A.; Zhang, Z.; Geller, S.; Tölke, J.; Krafczyk, M.; Meyer, D. The effect of the microfluidic diodicity on the efficiency of valve-less rectification micropumps using lattice boltzmann method. *Microsyst. Technol.* **2009**, *15*, 1379–1387. [[CrossRef](#)]
67. Yang, B.; Lin, Q. Planar micro-check valves exploiting large polymer compliance. *Sens. Actuator A Phys.* **2007**, *134*, 186–193. [[CrossRef](#)]
68. Yang, B.; Lin, Q. A planar compliance-based self-adaptive microfluidic variable resistor. *J. Microelectromech. Syst.* **2007**, *16*, 411–419. [[CrossRef](#)]
69. Zhang, Q.; Peng, X.; Weng, S.; Zhang, R.; Fang, D.; Zhao, R.; Qi, H.J. Self-adaptive flexible valve as passive flow regulator. *Extreme Mech. Lett.* **2020**, *39*, 100824. [[CrossRef](#)]
70. Groisman, A.; Quake, S.R. A Microfluidic rectifier: Anisotropic flow resistance at low reynolds numbers. *Phys. Rev. Lett.* **2004**, *92*, 094501. [[CrossRef](#)]
71. Tirtaatmadja, V.; Sridhar, T. A filament stretching device for measurement of extensional viscosity. *J. Rheol.* **1993**, *37*, 1081–1102. [[CrossRef](#)]

72. Landau, L.; Lifshitz, E. *Fluid Mechanics*, 2nd ed.; Pergamon Press: New York, NY, USA, 1987.
73. Oh, K.W.; Ahn, C.H. A review of microvalves. *J. Micromech. Microeng.* **2006**, *16*, R13–R39. [[CrossRef](#)]

**Publisher’s Note:** MDPI stays neutral with regard to jurisdictional claims in published maps and institutional affiliations.



© 2020 by the author. Licensee MDPI, Basel, Switzerland. This article is an open access article distributed under the terms and conditions of the Creative Commons Attribution (CC BY) license (<http://creativecommons.org/licenses/by/4.0/>).